

## Permafrost models intercomparison

M.M.Arzhanov<sup>1</sup>, O.A.Anisimov<sup>2</sup>, P.F.Demchenko<sup>1</sup>, A.V.Eliseev<sup>1</sup> and I.I.Mokhov<sup>1</sup>  
 (1) A.M.Obukhov Institute of Atmospheric Physics RAS, 3 Pyzhevsky, 119017  
 Moscow, Russia,  
 e-mail: [arzhanov@ifaran.ru](mailto:arzhanov@ifaran.ru)

(2) State Hydrological Institute, Second Line V.O., 23, 199053 St.Petersburg,  
 Russia,  
 e-mail: [oleg@oa7661.spb.edu](mailto:oleg@oa7661.spb.edu)

About 25 per cent of the total Northern Hemisphere land area is covered by permafrost. Here the preliminary results of the intercomparison of the models for permafrost evaluation are presented.

An intercomparison is performed for four particular models: integral permafrost model, IPM (Kudryavtsev et al., 1984), differential models developed at the State Hydrological Institute, SHI, (Anisimov, 1998), the State Hydrological Institute - A.M.Obukhov Institute of Atmospheric Physics RAS, SHI-IAP RAS (which is based on (Woelbroeck, 1993)) and at the Institute of Numerical Mathematics RAS, INM RAS (Volodina, 2001). The computations are made for a number of selected Russian sites where observational data for the last few decades exist: Yakutsk (62N 129E), Tiksi (72N 128E), Marre-Sale (69N 66E), Vorkuta (67N 64E) for different soil types. Meteorological variables are taken from the NCEP/NCAR reanalysis climatology (Kalnay et al., 1996) for 1979-1995.

The results of this intercomparison are presented in Table 1 and in Fig.1 The models show considerable scatter. As a whole the INM RAS model show larger seasonal thaw depths in comparison to other models.

This work is supported by the Russian Foundation for Basic Research and by the Russian President scientific grants.

Table 1: Seasonal thaw depths (in centimeters) for analyzed models in comparison to observations.

	Marre-Sale				Vorkuta				Yakutsk				Tiksi			
	INM RAS	IPM	SHI	SHI-IAP RAS	INM RAS	IPM	SHI	SHI-IAP RAS	INM RAS	IPM	SHI	SHI-IAP RAS	INM RAS	IPM	SHI	SHI-IAP RAS
loam	136	72	113	105	153	127	115	145	193	170	160	165	140	98	97	105
sand	157	88	120	118	204	155	122	160	263	207	174	175	156	118	100	110
clay	140	64	105	100	161	100	105	135	184	146	150	145	136	84	92	95
peat	76	24	49	30	64	82	48	35	131	41	65	45	72	76	46	27
observa tions	55 - 175				43 - 113				118 - 204				42 - 47			

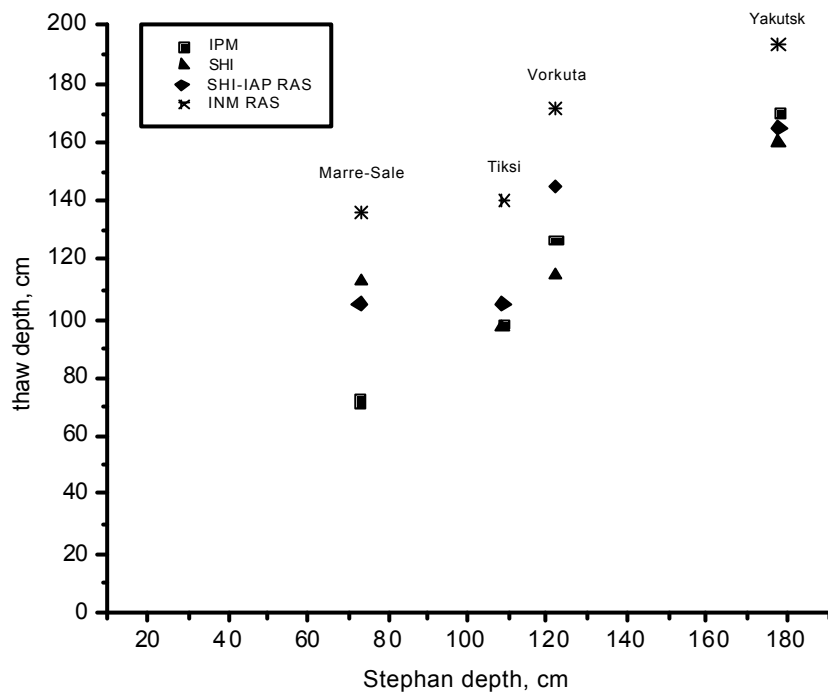


Fig.1: Seasonal thaw depths (in centimeters) for analyzed models as a function of the Stephan depth for loam soil type (see legend. Stephan depth is a seasonal thaw depth in the simplified soil thawing problem (Kudryavtsev et al., 1984).

#### Bibliography:

Anisimov O.A., 1998: Climate changes in the Northern Hemisphere cryolitizone and their impacts, Dr.Sci.Thesis. St.Petersburg State University, St.Petersburg, 37 p. [in Russian].

Kudryavtsev V.A., Garagulya L.S., Kondratyeva K.Ya., Melamed V.G., 1974: Basics of permafrost prediction for engineering-cryological studies. Nauka Publ. House, Moscow [In Russian].

Woelbroeck C., 1993: Climate-soil processes in the presence of permafrost: a systems modelling approach. *Ecol.Modelling*, 69 (1-2), 185-225.

Volodina E.E., 2001: Numerical study of sensitivity of hydrologic land surface characteristics to variations in physical parameters of the soil-vegetation-snow system. *Izvestiya, Atmos. Ocean. Phys.*, 37 (5), 651-660.

Kalnay E., and coauthors, 1996: The NCEP/NCAR 40-year reanalysis project. *Bull. Amer. Met. Soc.*, 77, 437--471.

## **Parameterization scheme for operational prediction of large-scale processes**

**Berkovich L. V., Tkacheva Yu.V.**

Hydrometeorological Research Center of Russia,  
e-mail: [berkovich@rhmc.mecom.ru](mailto:berkovich@rhmc.mecom.ru)

**Shnaydman V.A.**

Department of Environmental Sciences, State New Jersey University-Rutgers, USA  
e-mail: [volf@envsci.rutgers.edu](mailto:volf@envsci.rutgers.edu)

The current operational forecast models use the different parameterization schemes for horizontal and vertical turbulent exchange because their resolution is larger than the upper limit space scale of the inertial range with minus 5/3 behavior of the spectrum. The three-dimensional parameterization scheme is converted in two-dimensional one which is applied for horizontal turbulence description. The vertical turbulent exchange uses the boundary approximation, which simplifies the all turbulence closure equations and allows to represent the second moments in the characteristics of vertical profiles of the mean variables, turbulence kinetic energy and the length-scale.

The weakest link of turbulence parameterization options in current active models is probably the empirical length scale expression rather than the closure assumptions. The empirical approach to the length scale modeling doesn't allow to fulfill the physical requirements such as to restore the transfer the turbulence kinetic energy to the dissipation subrange through the buoyancy and inertial intervals of the spectrum under different stability conditions. The boundary approximation and the direct relationship from ground distance have no physical reason when the parameterization scheme is applied to atmosphere above the boundary layer.

The effective development of the vertical turbulent parameterization is connected with using the two-equation transport model, which involves the prognostic equations for turbulence kinetic energy and dissipation rate. The boundary layer model (BLM) is included in the large-scale prediction model of Russian Hydrometeorological Center (RHMC) operational prognostic model [Berkovich, L.V., Tarnopolskii, A.G., Shnaydman, V.A.]. The upper and lower boundary conditions for the boundary layer are taken from the large-scale prediction model. The explicit scheme of BLM time integration is applied by using the iteration procedure (3-5 iterations) on each time step.

The main achievements of the improved parameterization in RHMC operational model are the reconstruction of the transition from the nocturnal stable to daily convective boundary layer, increasing the dissipation rate when the stratification changes from stable to unstable, the recognition of the compound vertical profile of the turbulence coefficient in the convective boundary layer. Such features of boundary layer parameters behavior face difficulties when the operational weather prediction is performed by using only prognostic equation for turbulent kinetic energy and empirical formulae for length scale.

The experience of using two-equation parameterization scheme in the Russian Hydrometeorological Center operational prognostic model and confirms that the physical requirements to the turbulence description are fulfilled in this scheme.

As an example, the 24h and 36h forecast of nocturnal and daily vertical profiles of boundary parameters for Moscow at 03h and 15h, 15 July 2003 are given in the tables 1 and 2.

Table 1

z	t	dt/dz	V	dd	Kt	b*10	e*1000
[m]	[grad C]	grad/100m	Vmod		[m2/c]	[m2/c2]	[m2/c3]
0	19.52		0.0	0	0.004	3.000	93.8982
10	19.52	0.00	2.5	45	1.355	3.000	3.0544
20	19.42	-1.00	2.8	45	3.198	3.496	1.7580
30	19.30	-1.20	2.9	45	5.273	3.985	1.3850
50	19.07	-1.15	3.1	52	7.167	3.836	0.9444
100	18.63	-0.88	3.4	52	9.105	3.049	0.4697
150	18.35	-0.56	3.6	52	7.030	1.896	0.2353
200	17.95	-0.80	3.8	52	1.895	0.600	0.0873
250	17.49	-0.92	4.7	57	0.392	0.281	0.0927
300	17.01	-0.96	5.4	66	0.105	0.078	0.0269
350	16.73	-0.56	5.2	74	0.000	0.000	0.0000

Table 2

0	28.90		0.00	0	0.012	5.413	227.5590
10	28.62	-2.80	3.05	41	1.887	5.413	13.4202
20	28.30	-3.20	3.31	41	4.635	7.132	9.1162
30	28.17	-1.31	3.44	41	7.696	8.271	8.0005
50	28.06	-1.22	3.55	48	13.336	9.737	6.3985
100	27.47	-1.16	3.75	53	25.136	10.335	3.8244
150	26.93	-1.08	3.87	53	30.451	9.636	2.7445
200	26.41	-1.04	3.97	53	30.072	8.159	1.9921
250	25.99	-0.82	4.05	53	27.641	6.677	1.4518
300	25.52	-0.94	4.13	53	18.798	4.286	0.8795
350	24.71	-1.62	4.41	54	3.327	1.252	0.4244
400	23.72	-1.98	5.28	62	0.557	0.430	0.3131
450	22.76	-1.92	5.94	72	0.183	0.172	0.1358
500	21.60	-2.32	5.88	82	1.596	0.030	0.0365
550	20.81	-1.59	5.63	84	1.596	0.030	0.0291
600	19.75	-2.11	5.75	85	2.384	0.031	0.0001
650	18.99	-1.52	5.91	85	2.384	0.031	0.0001
700	18.50	-0.99	5.43	85	2.384	0.031	0.0001
750	17.34	-2.31	4.96	85	2.384	0.031	0.0001
800	16.70	-1.29	4.88	85	2.384	0.029	0.0001
900	15.89	-0.81	4.69	84	1.621	0.029	0.0001

Reference:

Berkovich, L.V., Tarnopolskii, A.G., Shnaydman, V.A.: 1997, "A Hydrodynamic Model of the Atmospheric and Oceanic Boundary Layers," Russian Meteorology and Hydrology 7, 30-40.

Berkovich, L.V., Tarnopolskii, A.G., Shnaydman, V.A.: 1997, "A Hydrodynamic Model of the Atmospheric and Oceanic Boundary Layers," Russian Meteorology and Hydrology 7, 30-40.

## The method of parameterization of convective cloudiness calculations

**Berkovich L. V.**

Hydrometeorological Research Center of Russia,  
**e-mail:berkovich@rhmc.mecom.ru**

Within the framework of hydrodynamical methods of weather forecast cloudiness has been calculated in the lower, middle and upper levels as one of the principal elements of the forecast. The mentioned cloudiness, which has non-convective character, is the main type of cloudiness forming with the development of large-scale processes due to the evolution of a humidity field of synoptic scale. At the same time in the middle and high latitudes, where Russia is situated, during the warm season the originating cloudiness comprises a substantial part of cloudiness of convective type, which is often accompanied by shower-type precipitation of considerable intensity. Direct calculation of convective cloudiness has been carried out in mesoscale models. In hydrostatic models that describe synoptic processes convective cloudiness can be calculated using parameterization methods. In the algorithm we have implemented the index of convective instability (ICN)  $B$  is first calculated:

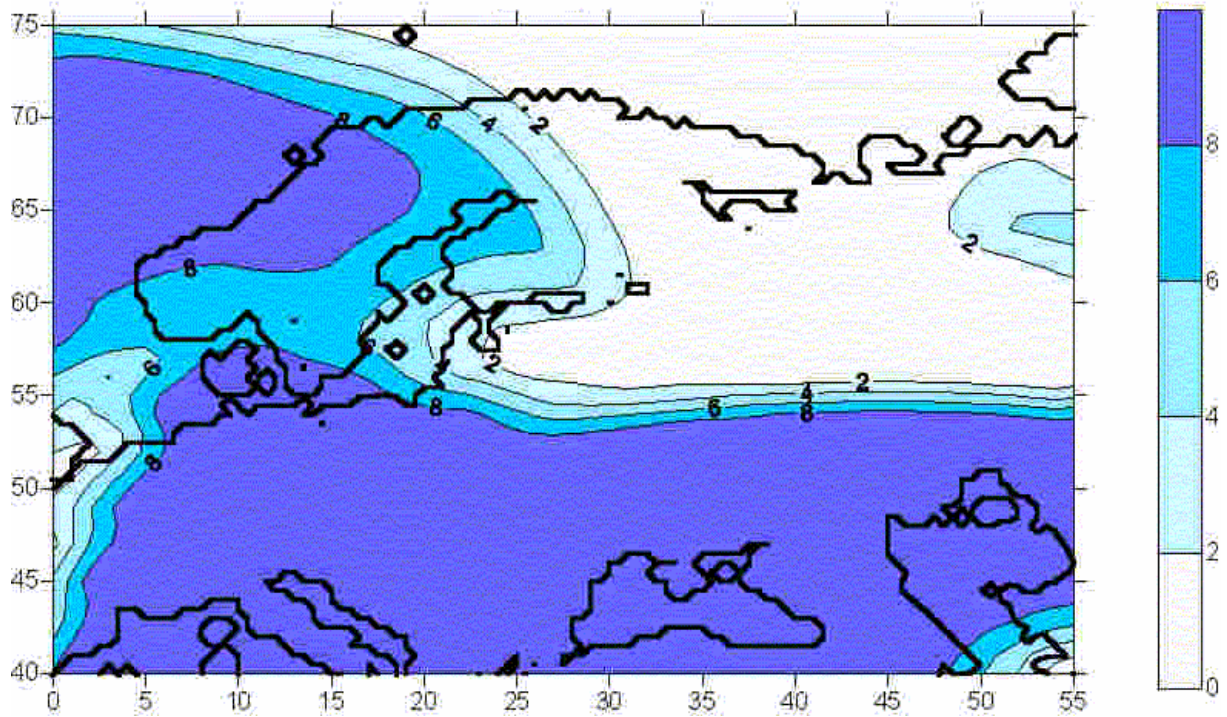
$$B = T_2 - T_K - \sum_{k=1}^K d_k, \quad d_k = T_k - T_{dk},$$

where  $T_2$  is the temperature at the level 2 m,  $T_K$  is the temperature at the surface 500 hPa,  $d_k$  is the dew-point  $T_{dk}$  deficit, and the levels of 2 m, 925, 850, 700, 500 hPa heights correspond to the values of  $k = 1, 2, \dots, K$ . The index  $B$  is the modified Whiting stability index, strongly differing nevertheless from the latter one by the fact that prognostic meteorological magnitudes at the levels 2 m and 925 hPa are taken into account. These data are of great importance, since one takes into account the distribution of temperature and humidity in the lower atmospheric layers, where the overwhelming amount of water vapour is grouped. To calculate the ball of convective cloudiness, the following scheme was suggested:

$$N = \frac{B - B_{cr}}{B_{max} - B_{cr}},$$

Here  $B$  is the current value of ICN,  $B_{cr}$  is the value of  $B$  at which the development of convective cloudiness begins (at  $B \leq B_{cr}$   $N = 0$ ), at  $B \geq B_{max}$  convective cloudiness is maximal,  $N = 1$ . The parameters  $B_{cr}$  and  $B_{max}$  vary for different geographic regions and different months of the warm season. These values are obtained empirically. For the Moscow area their means are as follows:  $B_{cr} = 27$ ,  $B_{max} = 37$ . Fields of convective cloudiness have been calculated using the procedure described above. Convective cloudiness is not measured separately. How successful will be its calculation may be estimated by the amount of shower-type precipitation that has fallen and which is measured at a network of meteorological stations. Since in the formula for the cloudiness ball calculation the large-scale parameters are determined using meteorological fields of synoptic scale, the convective cloudiness correlates with the non-convective cloudiness fields. (To efficiently calculate local convective clouds mesoscale models of the atmosphere have to be used.) Such convective-type cloudiness of 8 – 10 balls ( $N = 0.8 \div 1.0$ ) is often accompanied by moderate and heavy shower-type precipitation. The illustration presents the convective cloudiness field forecast for 36 h using the initial data of 8 July 2003 00 h UTC. It is presented in the form of colored background, in accordance with the given scale. This 36-h forecast corresponds to the diurnal period, when convective cloudiness actively develops. The characteristic features of the synoptic situation were a trough over Scandinavia, cyclones with the centers over the Mediterranean Sea and the Caucasus; over the rest of the Eastern Europe territory an area of high pressure was situated. In the region of Moscow within the period under investigation considerable amount of

precipitation has fallen (15 – 35 mm per day), with a substantial share of shower rains, which is connected with the development of convective cloudiness. In particular, at the Moscow stations “Exhibition Center” and “Izmailovo” major amount of precipitation has fallen (27 and 38 mm a day, respectively), and at the station “Tushino” the lightest precipitation was observed (9 mm a day). In the average at the territory of Moscow the amount of diurnal precipitation was about 18 mm.



The convective cloudiness field forecast at 36 h.  
Initial data for 8 July 2003 00 h UTC

# A Sea Surface Stress Parameterization Dependent on Directional Sea State

Mark A. Bourassa<sup>1,2</sup>

(bourassa@coaps.fsu.edu)

1. Center for Ocean-Atmospheric Prediction Studies, Florida State University, Tallahassee, FL 32306-2840, USA

2. Department of Meteorology, Florida State University, Tallahassee, FL 32306-4520, USA

## 1. INTRODUCTION

A physically based model is developed for the dependency of surface turbulent stress on directional wave characteristics. The physical impacts of sea state are parameterized through the influences of the surface's orbital motion induced by waves. Such a model has been successfully applied to capillary-wave related surface stress (Bourassa *et al.*, 1999); however, such wave dominate stress for ten meter wind speeds ( $U_{10}$ )  $< \sim 5$  ms<sup>-1</sup>. The mechanism was not applied to gravity wave related surface stresses, which dominate greater wind. A minor improvement (10% reduction in RMS differences) over Bourassa (2004) is made through a more detailed consideration of the lower boundary condition in the modified log-wind profile. Another advantage of this physically-based mechanism is that it considers directional sea state (i.e., the wind direction relative to the direction of wave propagation).

## 2. DATA

A preliminary version of observations from the Storm Wave Study experiment (SWS-2; Dobson *et al.*, 1999; Taylor *et al.*, 1999) was kindly provided by Peter K. Taylor. These observations were gathered in the North Atlantic Ocean, with the goal of gathering a high quality data set for severe wind conditions. The constraints applied for quality assurance are discussed in Bourassa (2004).

## 3. FLUX MODEL

The downward momentum flux ( $\tau$ ) can be modeled in terms of the friction velocity ( $\mathbf{u}_*$ ):

$$\tau = \rho \mathbf{u}_* |\mathbf{u}_*|, \quad (1)$$

where  $\rho$  is the density of the air. The influence of surface waves on stress is usually determined by the relation between  $\mathbf{u}_*$  and roughness length ( $z_o$ ). The modified log-wind relation is

$$\mathbf{U}(z) - \mathbf{U}_s = \frac{\mathbf{u}_*}{\kappa} \left[ \ln \left( \frac{z-d}{z_o} + 1 \right) + \varphi(z, z_o, L) \right], \quad (2)$$

where  $\mathbf{U}$  is the wind vector at height  $z$  above the local mean surface,  $k$  is von K arm an's constant,  $d$  is the

displacement height (the height at which the log wind profile extrapolates to zero wind speed), and  $L$  is the Monin-Obukhov stability length. The influence of atmospheric stratification in the boundary-layer is modeled through the Monin-Obukhov stability length. The parameterization of  $L$  is identical to that used in the BVW (Bourassa-Vincent-Wood) flux model (Bourassa *et al.*, 1999).

### 3.1 Momentum Roughness Length

The form of the momentum roughness length parameterization (3) used herein (Bourassa 2004) is a modification of BVW (Bourassa *et al.* 1999). This roughness length (Bourassa 2004) can be written with no explicit dependence on sea state, where the gravity wave roughness length is a two-dimensional version of Charnock's equation (Charnock, 1955). The influence of sea state on stress enters solely through the modification of vertical shear in wind speed (4), due to a non-zero lower boundary condition: the wave-induced surface motion. The roughness length is anisotropic, with unit vectors parallel ( $\hat{e}_1$ ) and perpendicular ( $\hat{e}_2$ ) to the mean direction of wave motion. It considers contributions to surface roughness from three types of surface features

$$z_o = \beta'_v \frac{0.11\nu}{|\mathbf{u}_*|} + \left[ \left( \beta'_c \frac{b \sigma}{\rho_w |\mathbf{u}_*| |\mathbf{u}_* \cdot \hat{e}_1|} \right)^2 + \left( \beta'_g \frac{a |\mathbf{u}_*| |\mathbf{u}_* \cdot \hat{e}_1|}{g} \right)^2 \right]^{0.5} \quad (3)$$

where the  $\beta$  terms are binary weights for the roughness lengths associated with (from left to right, an aerodynamically smooth surface, capillary waves, and gravity waves), where  $\nu$  is the molecular viscosity of air,  $b$  is a dimensionless constant (determined from laboratory observations; Bourassa *et al.* 1999),  $\sigma$  is surface tension,  $\rho_w$  is water density,  $c_p$  is the phase speed of the dominant waves, and  $g$  is gravitational acceleration. The orbital velocity ( $U_{orb}$ ) changes the velocity frame of reference to that of a fraction  $f$  of the orbital velocity of the dominant waves. Laboratory

studies (Okuda *et al.*, 1997) have shown that most of the interactions between wind and waves occur near the crest of the dominant waves).

$$\left[ \mathbf{U}(z) - f\mathbf{U}_{orb} - \mathbf{U}_{current} \right] \bullet \hat{\mathbf{e}}_i = \frac{\mathbf{u}_* \bullet \hat{\mathbf{e}}_i}{\kappa} \left[ \ln \left( \frac{z-d}{z_o} + 1 \right) + \varphi(z, z_o, L) \right] \quad (4)$$

The orbital speed of gravity waves is approximated by

$$U_{orb} = \pi H_s / T_p \quad (5)$$

where  $H_s$  is the significant wave height, and  $T_p$  is the period of the significant waves. The fraction of the orbital velocity ( $f$ ) that modifies the surface condition was set at 80% (Bourassa 2004). Herein, a non-zero displacement height is considered. The displacement height, 60% of the significant wave height, is determined by assuming circular orbital motion and a height corresponding to a horizontal velocity of 80% of the orbital velocity. Consideration of displacement height reduced the rms difference by almost 10%. Charnock's constant is highly dependent on the velocity frame of reference ( $f\mathbf{U}_{orb} - \mathbf{U}_{current}$ ) and displacement height ( $d$ ): a small change in  $|\mathbf{u}_*|$  corresponds to a large percentage change in  $z_o$ . This approach reduced the root-mean-square (rms) differences between modeled and observed friction velocity from 0.078 to 0.041  $\text{ms}^{-1}$ . Without displacement height, it was found that  $a = 0.064$  resulted in an excellent fit to the SWS2 data. Herein, considering  $d$ , results in  $a = 0.035$ , and improves the fit for the highest wind speeds (fig. 1).

The lack of wave directional information in the preliminary release of the SWS2 data, and hence the lack of consideration in this study, presumably accounts for a substantial fraction of the unaccounted for variability in the SWS2 data.

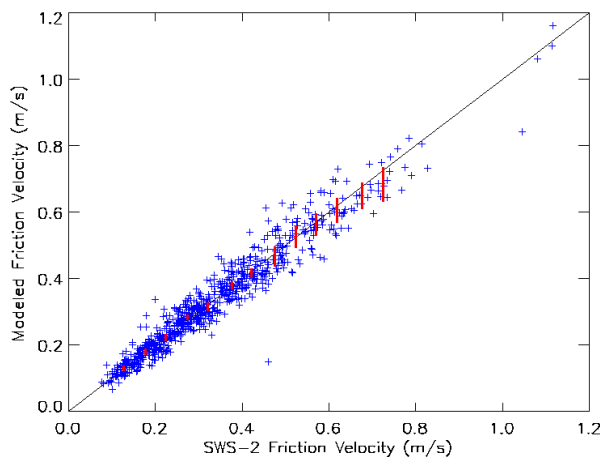


Fig. 1. Comparison of modeled and observed friction velocity magnitudes. The observations are from the SWS2 experiment. The red bars are centered on the mean, and extend for  $\pm$  standard deviations in the mean.

#### 4. COMPARISONS TO OBSERVATIONS

The model is evaluated with SWS-2 observations, as this data set is deemed the best for calibration purposes. In particular, all the required meteorological data, flux data, and wave data were recorded (however, wave directional information is not available at this time), and the surface water is well mixed, allowing the differences between bulk and skin temperature to safely be ignored.

The comparison (fig. 1) to the SWS2 friction velocity observations is good, particularly in the mean. The rms difference between modeled and observed values is 0.041  $\text{ms}^{-1}$  when the orbital velocity and displacement height are considered, and increases to 0.078  $\text{ms}^{-1}$  when these considerations are ignored (and  $a$  is tuned accordingly). The median value of the absolute value of the relative error is 11% when orbital velocity and displacement height are considered.

**Acknowledgments.** I thank Peter Taylor for providing the SWS-2 data and advice on quality assurance. COAPS receives its base funding from ONR's Secretary of Navy Grant to James J. O'Brien. Support is from OSU's SeaWinds project, the Florida State University's FYAP program, and the NSF.

#### REFERENCES

- Bourassa, M. A., 2004: An Improved Seastate Dependency For Surface Stress Derived from In Situ and Remotely Sensed Winds. *Advances in Space Res.*, in press.
- Bourassa, M. A., D. G. Vincent, and W. L. Wood, A flux parameterization including the effects of capillary waves and sea state. *J. Atmos. Sci.*, **56**, 1123-1139, 1999.
- Charnock, H., Wind stress on a water surface. *Quart. J. Roy. Meteor. Soc.*, **81**, 639-640, 1955.
- Dobson, F. W., R. J. Anderson, P. K. Taylor, and M. J. Yelland, Storm Wind Study II: Open ocean wind and sea state measurements. *Proc. Symp. on the Wind-Driven Air-Sea Interface: Electromagnetic and Acoustic Sensing, Wave Dynamics and Turbulent Fluxes*, M. L. Banner, Ed., University of New South Wales, 295-296, 1999.
- Okuda, K., S. Kawai, and Y. Toba, 1997: Measurements of skin friction distribution along the surface of wind waves. *J. Oceanog. Soc. Japan*, **33**, 190-198.
- Taylor, P. K., and M. J. Yelland, F. W. Dobson, R. J. Anderson, Storm Wind Study II: Wind stress estimates from buoy and ship. *Proc. Symp. on the Wind-Driven Air-Sea Interface: Electromagnetic and Acoustic Sensing, Wave Dynamics and Turbulent Fluxes*, M. L. Banner, Ed., University of New South Wales, 353-354, 1999.

# Comparison of surface models CLASS and ISBA over North America

**Yves Delage, Stéphane Bélair,**  
Recherche en prévision numérique (RPN),  
Meteorological Service of Canada, Dorval, Quebec, Canada  
[yves.delage@ec.gc.ca](mailto:yves.delage@ec.gc.ca)

**Carole Labadie and Émilie Mallet**  
École Nationale de la Météorologie  
Météo-France

=====  
**Context**

The Canadian land-surface model CLASS and the French model ISBA were run in parallel from 1 May 2002 to 31 March 2003 over North America at a resolution of 10 km. Both models were forced by the same meteorological input (downward radiative fluxes, precipitation, and temperature, wind and humidity at ~ 40 m) from a series of 24 hour forecasts from the operational model at the Canadian Meteorological Centre (CMC). The surface fluxes produced by each model did not feed back on the atmospheric model (off-line mode).

**Similarity and differences between the models**

The ISBA model is the version present in the operational forecast model at CMC, while CLASS is version 3.0 but without the mosaic capability, the new sloping terrain runoff parameterization and without organic soils. A maximum number of common parameters were given to both models to minimize the differences between them. Vegetation and soil types, vegetation roughnesses and albedos as well as the thicknesses of permeable soil were identical. Leaf area indices, vegetation fractions and initial values of temperature and soil moisture were very close.

Despite the efforts to make both models share the same parameters, structural and formulation differences remained. The principal differences are listed here.

*Surface temperature and energy budget:* CLASS makes distinct calculations for vegetation and bare ground, and for snow covered and snow free portions of each grid point; ISBA makes a single calculation.

*Heat and moisture vertical transfers in the soil:* CLASS uses a diffusion equation and Darcian equations with three soil layers while ISBA uses a 'force-restore' approach with the diurnal time scale for both variables.

*Stomatal resistance:* ISBA uses a linear function of soil moisture content between the wilting point and the field capacity for modeling the effect of soil water while CLASS uses an exponential function, giving less resistance to transpiration for low and moderate soil moisture contents.

*Infiltration and runoff:* ISBA uses the VIC (Variable Infiltration Capacity) model while CLASS uses the Green-Ampt approach with surface ponding. Frozen soil impedes infiltration in CLASS but not in ISBA.

*Thawing and freezing of ground water:* This process is not handled conservatively in ISBA, underestimating its impact on soil temperature.

*Water reservoirs:* ISBA has a liquid water reservoir on the canopy while CLASS holds both rain water and snow. CLASS has a liquid water reservoir at the surface (ponding), three liquid and three solid ground water reservoirs while ISBA has two liquid and one solid water reservoirs in the ground. On the other hand, ISBA has a liquid water reservoir in the snow, which CLASS does not have yet.

## Results

Results indicate larger runoff in ISBA, except that due to snow melting over frozen soil. This is due in part to the large value of the form parameter ( $b=1.0$ ) used by ISBA in its infiltration model. This larger runoff resulted in generally smaller soil water contents in ISBA and hence smaller evapotranspiration rates. The difference in the formulation of the stomatal resistance (see above) also contributes to larger evapotranspiration in CLASS. There are areas, however, where ISBA evaporates more than CLASS. These are over warm and wet grounds, where it was found that bare soil evaporation is considerably larger in ISBA due to the large roughness length that it shares with the rest of the grid tile; in CLASS a separate (smaller) value of roughness is assigned to bare soil and the corresponding evaporation is smaller.

Snowmelt is slower in ISBA, partly because ISBA retains liquid water in the snow, which can refreeze at night, but also because it allows more sublimation than CLASS. This extra sublimation (which takes much more energy than melting and thus reduces snowmelt) is due to larger than zero Celsius temperature in ISBA in the snow, an unrealistic feature of the model.

Differences are also found in nighttime surface temperature during fall due to a combination of two factors. The force-restore scheme in ISBA handles reasonably correctly the diurnal cycle but completely ignores the annual (or seasonal) cycle. In particular, the upward ground heat flux during the fall coming from a warmer deep layer is missing and this contributes to cooler temperatures at the surface than with CLASS. The other factor is the underestimation in ISBA of the heat released by the freezing of ground water, which also contributes to lower the temperature at the surface during ground freezing episodes. The reverse effect should be found during spring but limitations in our experimental setup did not allow us to see it.

## Conclusions

ISBA and CLASS generally gave similar results but differences in structure and in formulation are reflected in the results. While the latter can easily be modified (for example the stomatal resistance formulation), structural features such as the internal mosaic of CLASS or the 'force-restore' of ISBA keep each model different from the other.

## Reference

Labadie, C. and É. Mallet, 2003: ``Comparaisons des modèles de surface ISBA et CLASS du 1<sup>er</sup> mai 2002 au 1<sup>er</sup> mars 2003 au-dessus de l'Amérique du Nord``, Rapport de stage, Recherche en prévision numérique, Service Météorologique du Canada, Dorval, Québec.

[http://www.cmc.ec.gc.ca/rpn/publications/pdf/Mallet\\_Labadie\\_rapport\\_de\\_stage\\_2003](http://www.cmc.ec.gc.ca/rpn/publications/pdf/Mallet_Labadie_rapport_de_stage_2003)

# Improvement of Microphysical Parameterization in a Japan Meteorological Agency Nonhydrostatic Model with a High Resolution and Its Effect on Simulation Result.

Akihiro HASHIMOTO<sup>2</sup>, Masataka MURAKAMI<sup>1</sup>, Teruyuki KATO<sup>1</sup>, Chiashi MUROI<sup>1</sup>, Masanori YOSHIZAKI<sup>1</sup>, Syugo HAYASHI<sup>1</sup>

<sup>1</sup>Meteorological Research Institute / Japan Meteorological Agency, Tsukuba

<sup>2</sup>Advanced Earth Science and Technology Organization, Tokyo

## 1. Introduction

We are developing a regional climate model with several kilometers mesh on the basis of JMA-NHM (Japan Meteorological Agency NonHydrostatic Model; Saito et al., 2001) in order to examine the change of precipitation intensity around Japan under the situation of global warming, and finally to contribute to IPCC (Kato et al. 2004). Microphysical processes are important for this purpose, because they affect the accuracy of prediction. Some improvements have been made on the microphysical parameterizations which are related to liquid hydrometeors in the model. We also performed a simulation of low-level stratocumulus clouds to examine the properties of improved parameterization, as a preliminary output for the climate prediction.

## 2. Improvements of microphysics in JMA-NHM

The microphysical processes in JMA-NHM are formulated with a bulk parameterization composed of three solid and two liquid water categories. The ice, snow, and graupel categories are represented by a 2-moment parameterization which has two prognostic variables, mixing ratio  $Q$  and number concentration  $N$ , to determine size spectra of hydrometeors. However, the cloud and rain categories were represented by a 1-moment parameterization which uses only  $Q$ . This old scheme is reformed so as to have 2-moment parameterization for cloud and rain in this study.

The old scheme assumes a size spectrum of cloud droplets to be mono-dispersion with constant number concentration  $10^8 \text{ m}^{-3}$ , while an exponential function is applied as a rain drop size spectrum. On the other hand, a new introduced scheme uses gamma functions to represent the size spectra of cloud droplets and rain drops, so as to make them more realistic. Figure 1 shows examples of those size spectra in the new and old schemes.

The new scheme has the following improvements in microphysical processes, compared with the old one. Some processes of warm rain such as auto-conversion, accretion of cloud droplets, and self-collection and breakup of rain drops are introduced based on Cohard and Pinty (2000). Increment of number concentration of cloud droplets

\*Corresponding author address: Akihiro Hashimoto, Meteorological Research Institute, 1-1 Nagamine, Tsukuba, Ibaraki 305-0052 Japan; e-mail: ahashimo@mri-jma.go.jp

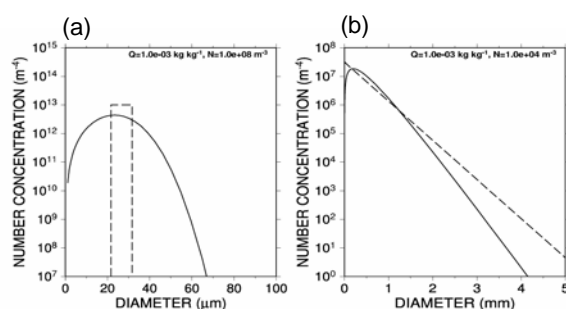


Fig. 1 Size spectra for (a) cloud droplets and (b) rain drops. Solid and broken lines correspond to those in the new and old schemes, respectively.

due to CCN (Cloud Condensation Nuclei) activation is diagnostically calculated based on the maximum super-saturation estimated with updraft velocity. The terms of the interaction with solid hydrometeors are modified so as to reflect the improvements of size spectra of cloud droplets and rain drops.

## 3. Numerical experiments

Figure 2 shows the model domain of 1-km horizontal resolution with the area of  $640 \times 640 \text{ km}^2$ . Vertically, 36 layers with variable intervals of 50 m to 220 m are employed. The model top is located at 4.7 km. The domain covers around the sea off the coast of Sanriku, the Tohoku, Japan. In this region, the low-level stratocumulus clouds often appear in the cold air mass flowing on relatively warm sea from the northern high pressure in summer. Integrated time interval is 5 s. The integration is conducted up to 8640 time steps (12 hours). Regional analysis data of JMA are referred as the boundary condition every hour. Initial time is 2100 JST, 1 Aug, 2001.

According to IR image of GMS, low-level clouds covered the sea off the coast of Sanriku at the present and the next days. We consider only warm rain process, because the targeted low-level stratocumulus clouds contain no ice particle.

Simulations with the new and old microphysical schemes are conducted to study the effect of the reformulations in microphysics on the model results.

## 4. Simulation results

The low-level stratocumulus clouds simulated by the model covers about  $40000\text{-km}^2$  area with the cloud base at about 300-m height and the cloud top at about 600-m height. For both simulations with the new and

old schemes, the amplitudes of vertical velocity are within 0.3 m/s, and the mixing ratios of cloud water are around 0.1 g/kg. A difference between the two schemes is apparent in the amount of rain water. Figure 3 shows the mixing ratio of rain water at 570-m height. The simulation with the new scheme produces rain water much more than the old one.

Figure 4 shows the relations between mixing ratio, and number concentration in the different ranges of mean-volume diameter. As shown in Figs. 4a and 4b, the new scheme produces large variations in the number concentration of cloud droplets  $N_{cw}$ , although the old scheme assumes no variation in  $N_{cw}$ . This result indicates that the new scheme can give the larger maximum values of mean-volume diameter (Fig. 4a), and that the new scheme can make the value of auto-conversion rate larger than the old one. Additionally, the number concentration of rain drops  $N_r$  is generally much larger for the new scheme, as shown in Figs. 4c and 4d. This enhances the accretion of cloud droplets by rain drops. Therefore, the new scheme produces the greater amount of rain water.

### 5. Summary

The microphysics in JMA-NHM has been improved with respect to the liquid hydrometeors. Its effect was examined in the simulations with low-level stratocumulus clouds in summer.

The new scheme modified the rain water distribution when it is compared with the old scheme. The new scheme produced greater values of the mixing ratio of rain water. This is due to the greater variations in number concentration of  $N_{cw}$  and  $N_r$  which are produced in a prognostic manner in the new scheme. The variation in  $N_{cw}$  accelerates auto-conversion, and that in  $N_r$  enhances the accretion of cloud droplets by rain drops.

### Acknowledgements

This study is conducted by the fund of Research Revolution 2002, and the numerical calculations are made by NEC SX-6 on the Earth Simulator.

### References

- Cohard, J. M. and J. P. Pinty, 2000: A comprehensive two-moment warm microphysical bulk scheme. I: Description and tests. *Q. J. R. Meteor. Soc.*, **126**, 1815-1842.
- Kato, T., K. Yasunaga, C. Muroi, M. Yoshizaki, A. Hashimoto, Y. Wakazuki, H. Eito, S. Hayashi and H. Sasaki, 2004: Regional Climate Prediction by using a Japan Meteorological Agency Nonhydrostatic Model with a High Resolution. Part 1: Outline/Purpose of a High-Resolution Long-Term Prediction. *CAS/JSC WGNE Research Activities in Atmospheric and Oceanic Modeling*, submitted.
- Saito, K., T. Kato, H. Eito and C. Muroi, 2001: Documentation of the Meteorological Research Institute / Numerical Prediction Division Unified Nonhydrostatic Model. *Tech. Rep. of MRI*, **42**, p133.

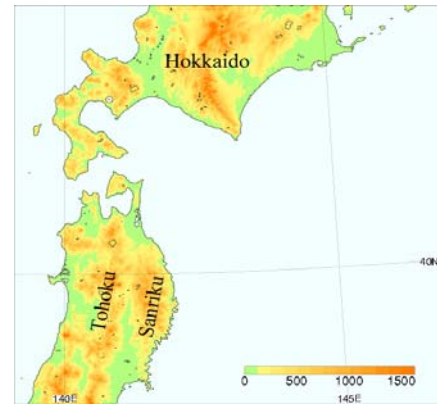


Fig. 2 The model domain and orography.

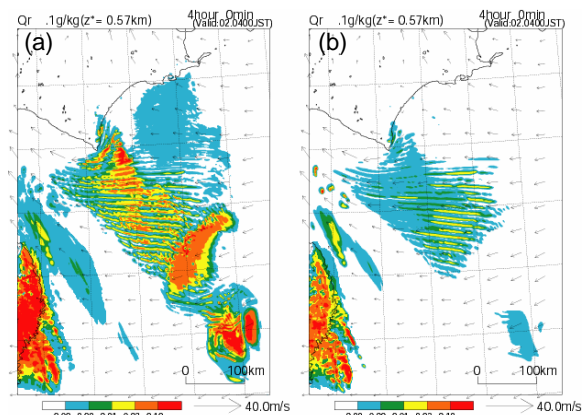


Fig. 3 Mixing ratio of rain water for (a) new and (b) old schemes at 570-m height.

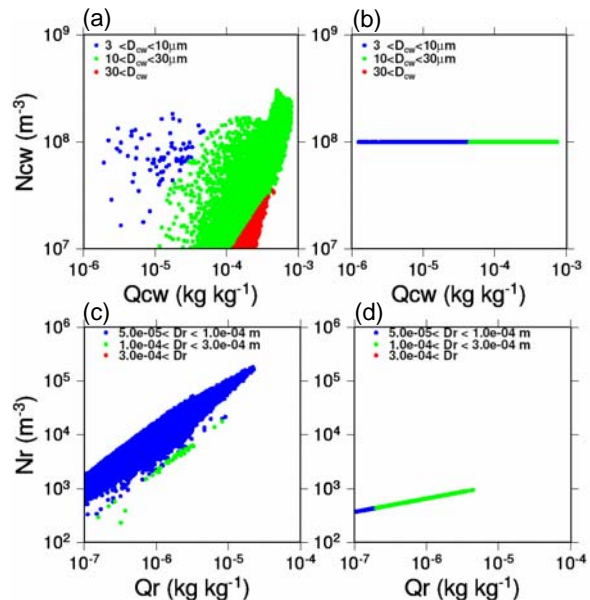


Fig. 4 Relations between mixing ratio  $Q$  and number concentration  $N$  in the different ranges of mean-volume diameter  $D$  which are shown by colors. (a) and (b) indicate the relations for cloud water, while (c) and (d) indicate those for rain water. (a) and (c) correspond to the results with new scheme, and (b) and (d) correspond to those with old scheme.

# Impact of a Parameterization for Subtropical Marine Stratocumulus

Hideaki Kawai

Climate Prediction Division, Japan Meteorological Agency

(e-mail: [h-kawai@met.kishou.go.jp](mailto:h-kawai@met.kishou.go.jp))

## 1. Background

It is very difficult to represent a subtropical marine stratocumulus off the west coasts of the continents in General Circulation Models (GCMs) because of its complicated physical interactions in and around the clouds and a lack of vertical resolution of GCM. Therefore a lot of efforts have been devoted to simulate the clouds by model researchers. Those clouds have not been represented in Global Spectral Model (GSM) in JMA either where the prognostic cloud scheme by Sommeria and Deardorff (1977) is adopted.

## 2. Parameterization for Subtropical Marine Stratocumulus

Instead of detail consideration of total water and temperature fluctuation in the prognostic cloud scheme, the simple and classical parameterization by Slingo (1980, 1987) is implemented with some minor modifications. This is an exception of the prognostic cloud scheme.

The stratocumulus is formed in areas and layers where all following conditions are met.

- $-\frac{\partial J}{\partial P} > 0.07$  [K/hPa] (just above the layer)
- $-\frac{\partial J}{\partial P} < 0.01$  [K/hPa] (near the surface)
- the height of the layer is below 940 [hPa]

where  $q$  is potential temperature and  $P$  is pressure. The first condition guarantees the existence of strong inversion at the cloud top, the second one is to prevent the pseudo formation of stratocumulus in strong stable layer, for example, above land or sea ice in the nighttime and the last one is to intercept the fictitious development of stratocumulus in shallow convection area, where the altitude of inversion is higher.

The cloud amount  $C_L$  and cloud water content in cloud  $q_{cl}$  are determined as below.

$$C_L = 12.0 \left( -\frac{\partial J}{\partial P} - 0.07 \right)$$

$$q_{cl} = 0.03 q_{sat}$$

where  $q_{sat}$  represents saturation specific humidity. Note that water vapor is reduced by cloud water content to conserve total water.

An important process concerning stratocumulus is a cloud top entrainment (CTE) process. GSM uses local turbulence closure model by Mellor and Yamada (1982). But local turbulence scheme causes concentration of moisture and consequent excessive production of boundary layer cloud at the top of boundary layer because of the large difference of vertical diffusivity between above and below the top of boundary layer almost all over the oceans. To prevent this problem, some value of vertical diffusivity is added even at strong inversion layer. Namely it works like CTE. Therefore this treatment is made invalid if three conditions described above are met.

## 3. Result

The results of one-month integration for July 2001 are shown at Figure 1 and Figure 2. Figure 1 shows the cloud amounts of without (left) and with (right) a stratocumulus parameterization. Low cloud amount is remarkably and selectively increased in off California, off Peru, off Mauritania, off Namibia regions. Figure 2 shows correspondent errors of upward shortwave radiation at the top of the atmosphere in which ERBE (Earth

Radiation Budget Experiment) observation data are used as climatology. The serious negative biases caused by a lack of reflection due to stratocumulus in these regions are reduced. The positive bias in downward shortwave radiation on the surface and negative bias of downward longwave radiation on the surface are also improved (not shown). Figure 3 shows the comparisons of seasonal variation of stratocumulus for 1992 off California, off Peru, off Mauritania and off Namibia regions. The parameterization represents the observational variations of stratocumulus (Klein and Hartmann 1993) well. Diurnal variation of cloud amount and total cloud water content of the cloud are also consistent with observations (not shown).

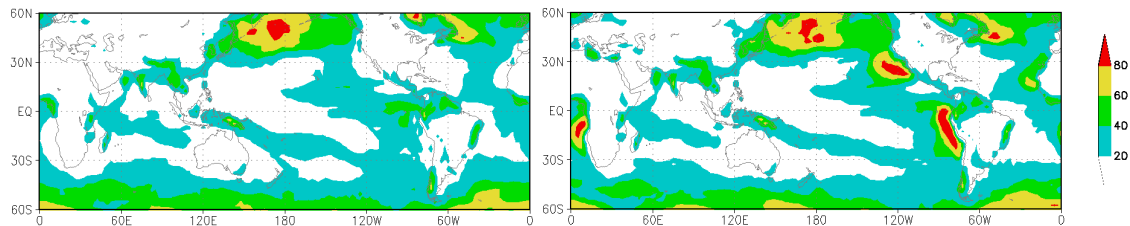


**Fig. 1:** Low cloud amounts in unit of [%] using T106 for July 2001 calculated left) without and right) with a stratocumulus parameterization.

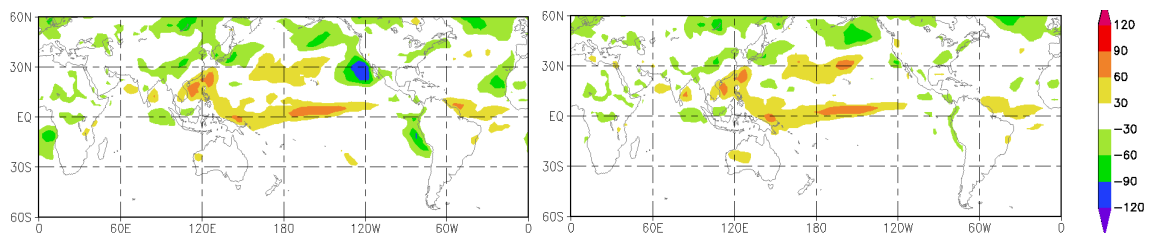


**Fig. 2:** As in Fig.1 but for errors of upward shortwave radiation at the top of the atmosphere [ $W/m^2$ ]. Errors are calculated based on ERBE observation data.

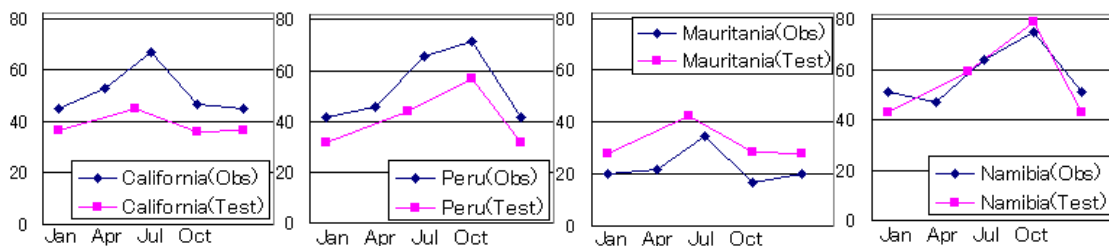


**Fig. 3:** Seasonal variations of stratocumulus cloud amount [%] using T63 for 1992 off California, off Peru, off Mauritania and off Namibia regions from left side. Observation data are from Klein and Hartmann (1993).

### References

- Klein, S. A., and D. L. Hartmann, 1993: The seasonal cycle of low stratiform clouds. *J. Climate*, **6**, 1587–1606.
- Mellor, G. L. and T. Yamada, 1982: Development of a turbulence closure model for geophysical fluid problems, *Rev. Geophys. Space Phys.*, **20**, 851–875.
- Slingo, J. M., 1980: A cloud parameterization scheme derived from GATE data for use with a numerical model. *Quart. J. Roy. Meteor. Soc.*, **106**, 747–770.
- Slingo, J. M., 1987: The development and verification of a cloud prediction scheme in the ECMWF model. *Quart. J. Roy. Meteor. Soc.*, **113**, 899–927.
- Sommeria, G., and J. W. Deardorff, 1977: Subgrid-scale condensation in models of non-precipitating clouds. *J. Atmos. Sci.*, **34**, 345–355.

# Fast and Accurate Approximation of the Long Wave Radiation Parameterization in a GCM Using Neural Networks: Evaluation of Computational Performance and Accuracy of Approximation in the NCAR Single Column Model

Vladimir M. Krasnopolsky,

Earth System Science Interdisciplinary Center, University of Maryland and SAIC at NCEP/NOAA, USA

Phone: 301-763-8000 x 7262, Fax: 301-763-8545, Email: [Vladimir.Krasnopolsky@noaa.gov](mailto:Vladimir.Krasnopolsky@noaa.gov)

Michael S. Fox-Rabinovitz, and Dmitry V. Chalikov

Earth System Science Interdisciplinary Center, University of Maryland, USA

A new approach using neural networks was applied to develop a fast and accurate approximation of atmospheric long wave radiation parameterization used in numerical climate and weather prediction models. The long wave radiation is usually the most time consuming part of model physics calculations.

NN approximations of model physics are based on the fact that any parameterization of physics can be considered as a continuous or almost continuous mapping (input vector vs. output vector dependence), and NNs are a generic tool for approximation of such mappings [Krasnopolsky and Chevallie, 2003]. NN is an analytical approximation that uses a family of functions like:

$$y_q = a_{q0} + \sum_{j=1}^k a_{qj} \cdot \phi(b_{j0} + \sum_{i=1}^n b_{ji} \cdot x_i); \quad q = 1, 2, \dots, m \quad (1)$$

where  $x_i$  and  $y_q$  are components of the input and output vectors respectively,  $a$  and  $b$  are fitting parameters, and  $\phi$  is a so called activation function (usually it is a hyperbolic tangent),  $n$  and  $m$  are the numbers of inputs and outputs respectively, and  $k$  is the number of neurons in the hidden layer (for more details see appendix in [Krasnopolsky et al., 2002]).

The function of the LW radiation parameterization in atmospheric GCMs is to calculate heat fluxes caused by LW radiation processes in the atmosphere. In the NCAR CAM LWR parameterization [Collins et al., 2002] used in this study, the calculations of cloudiness are completely separated from the calculations of radiation effects. Due to this structure convenient for NN approximation, we are able to approximate the entire LW radiation parameterization with only one NN, with cloudiness used just as one of the inputs of this NN.

The NN developed for approximation of the LW radiation parameterization has 101 inputs ( $n = 101$  in eq. (1)), which include seven profiles (atmospheric temperature, humidity, ozone concentration, path length for CO<sub>2</sub>, path length for H<sub>2</sub>O, and cloudiness) and two relevant surface characteristics (surface pressure and the upward LW flux at the surface). This NN has 19 outputs ( $m = 19$  in eq. (1)): a profile of the heat rates (HRs)  $\{q_k\}_{k=1, \dots, 18}$  and downward LW flux to the surface. The NN has one hidden layer with 90 neurons ( $k = 90$  in eq. (1)) that provide the sufficient accuracy of approximation.

For this initial experiment, a representative data set consisting of about 100,000 input/output combinations has been generated using the 19-level NCAR single column model with the physics identical to that of NCAR CAM-2. This model simulation data set covers the entire year of 2002. It was divided into three parts each containing about 33,000 input/output combinations. The first part was used for training, the second one was used for tests (control of overfitting, control of a NN architecture, etc.), and the third part was used for validations only.

Table 1 shows a bulk validation statistics for the accuracy of approximation and computational performance of our NN approximation and also the comparison with the accuracy and performance of the successful ECMWF NeuroFlux approximation [Chevallier et al., 2000]. NN approximations have been evaluated against the original parameterizations. For calculating the error

statistics presented in Table 1, the original parameterization and its NN approximation have been applied to validation data. Two sets of the corresponding HR profiles and two sets of outgoing long wave radiations (OLRs) (for the original parameterization and its approximation) have been generated. Bias (or the mean error) and RMSE presented in Table 1 have been calculated as the mean differences between these two sets of HRs and OLRs. Mean values and standard deviations ( $\sigma$ ) of HRs and OLRs are also presented for a better understanding of relative errors. The ECMWF results are also shown for comparison. Our NN approximation has very high accuracy with an almost negligible systematic error (bias). Most importantly, that in addition to that it performs 65 times faster than the original parameterization. This speed-up is achieved for NN approximation of the entire LW radiation scheme that includes calculations of optical properties (emissivity and absorptivity), and HRs and radiative fluxes.

*Table 1. Accuracy and Computational Performance of LW NN Approximation for NCAR CAM-2 and the ECMWF Model vs. their Corresponding Original Parameterizations*

Parameter	Model	Bias	RMSE	Mean	$\sigma$	Performance
HR (K/d)	ECMWF	0.2	0.45			8 times faster
	NCAR	0.00002	0.05	-1.43	1.76	65 times faster
OLR ( $W/m^2$ )	ECMWF	0.8	1.9			
	NCAR	0.01	0.9	240.5	46.9	

The obtained results show that the NN approximation of the considered atmospheric LW radiation parameterization is highly accurate and provides a significantly improved computational efficiency. It opens the opportunity of a complete reexamination of computations for all model physics components in NCAR CAM. This in turn will potentially make an important positive impact on extensive experimentation with this kind of complex models needed for improving climate change assessments and weather prediction. The developed methodology can be applied to other LW radiation schemes used in the variety of applications.

Currently, we are working on development of NN approximation of the LW radiation for NCAR CAM and producing climate simulation results using this NN approximation. The preliminary results show that the parallel NCAR CAM climate simulations, performed with the original LW radiation parameterization and its NN approximation, are very close to each other [Krasnopolsky *et al.*, 2004]. Results of this study will be submitted to the next issue of this report.

**Acknowledgments.** The authors would like to thank Drs. W. Collins, P. Rasch, and J. Tribbia for useful discussions and consultations.

Chevallier, F., J.-J. Morcrette, F. Chéruy, and N. A. Scott, “Use of a neural-network-based longwave radiative transfer scheme in the EMCWF atmospheric model”, *Quarterly Journal of Royal Meteorological Society*, 126, 761-776, 2000

Collins, W.D., J.K. Hackney, and D.P. Edwards, “A new parameterization for infrared emission and absorption by water vapor in the National Center for Atmospheric Research Community Atmosphere Model”, *J. Geophys. Res.*, 107 (D22), 2002

Krasnopolsky, V.M., and F. Chevallier, “Some neural network applications in environmental sciences. Part II: Advancing computational efficiency of environmental numerical models”, *Neural Networks*, 16, 335-348, 2003

Krasnopolsky, V.M., M.S. Fox-Rabinovitz, and D.V. Chalikov, “Fast and Accurate Neural Network Approximation of Long Wave Radiation in a Climate Model”, to be submitted, 2004

# Implementation of a non-local like PBL scheme in JMANHM

KUMAGAI Yukihiro

Numerical Prediction Division, Japan Meteorological Agency

1-3-4 Otemachi, Chiyoda, Tokyo 100-8122, Japan, [kumagai\\_y@met.kishou.go.jp](mailto:kumagai_y@met.kishou.go.jp)

The JMA non-hydrostatic model(JMANHM) is a community model which has been developed for use of both operational prediction and research. JMANHM is known to have several problems in the surface properties such as temperature and humidity:

**Problem 1** The cold bias at the surface in case of the unstable conditions.

**Problem 2** The wet bias at the surface.

The causes of the problems are the following points:

**Cause 1** Too much the surface latent heat flux.

**Cause 2** Too small the eddy diffusion coefficients.

The more the surface latent heat flux exists, the more surface cooling occurs. That is why the cold bias at the surface existed. Furthermore, because of the small turbulent mixing with the small eddy diffusion coefficients, the water vapor in the lower model level is accumulated too much. That is why the wet bias at the surface existed.

Kumagai[1] removed the Cause 1 and solved the Problem 1 by modifying the land surface processes, while the Problem 2 remained. To remove the Cause 2 and solve the Problem 2, the following modifications have been made.

## 1) Non-local like PBL scheme

The turbulent closure of JMANHM is 1.5-order TKE-based closure, and the eddy diffusion coefficients  $K_m, K_h$  are calculated as follows:

$$\frac{\partial E}{\partial t} = -ADV.E - \frac{gK_h}{\theta G^{\frac{1}{2}}} \frac{\partial \theta_l}{\partial z^*} - \sum_{i,j} \overline{u'_i u'_j} \frac{\partial u_i}{\partial x_j} - \frac{C_e E^{\frac{3}{2}}}{l} + DIF.E , \quad (1)$$

$$\overline{u'_i u'_j} = -K_m \left( \frac{\partial u_i}{\partial x_j} + \frac{\partial u_j}{\partial x_i} \right) + \frac{2}{3} \delta_{ij} E , \quad (2)$$

$$K_m = C_m l E^{\frac{1}{2}} , \quad K_h = \frac{1}{Pr} K_m , \quad (3)$$

$$l_\infty = \begin{cases} \Delta s & N^2 \leq 0 \\ \min(\Delta s, 0.76 \frac{E^{\frac{1}{2}}}{N}) & N^2 > 0 \end{cases} , \quad (4)$$

$$\frac{1}{l} = \frac{1}{k(z - z_s)} + \frac{1}{l_\infty} . \quad (5)$$

Here  $\Delta s$  is the grid scale. Obviously, the eddy diffusion coefficients  $K_m, K_h$  in Eq. (3) are strongly dependent on the mixing length  $l$ .

The mixing length  $l$  is regarded as the maximum scale of turbulence. So, at most the grid scale turbulence are considered by using Eq. (4). Furthermore, the mixing length  $l$  is restricted to the product of Kármán constant  $k$  and the height  $(z - z_s)$  by using Eq. (5). But, in a convective boundary layer, large eddies which have the scale of the PBL height exist and the atmosphere is mixed by these large eddies. To include the effect of the large eddies, a non-local like PBL scheme has been implemented into JMANHM following Sun and Chang[2]. The mixing length  $l$  below the PBL top is decided by using the PBL height  $h_{\text{PBL}}$  as follows:

$$l = 0.25 \left[ 1.8 h_{\text{PBL}} \left\{ 1 - \exp \left( -4 \frac{z - z_s}{h_{\text{PBL}}} \right) - 0.0003 \exp \left( 8 \frac{z - z_s}{h_{\text{PBL}}} \right) \right\} \right] . \quad (6)$$

By using Eq. (6) instead of Eqs. (4) and (5) below the PBL top, the mixing length  $l$  becomes larger. This leads to the increase of the eddy diffusion coefficients  $K_m, K_h$  through Eq. (3).

## 2) Anisotropy of turbulence

When the grid aspect ratio  $\Delta x / \Delta z$  is much larger than the order of unity, the turbulence can not be isotropic. Since the mixing length  $l$  is regarded as the maximum scale of turbulence, the mixing length has to be different values for the horizontal and vertical directions. So, an option for anisotropy of turbulence has been added to JMANHM. If this option is selected, the mixing length of the horizontal direction is set to be equal to the horizontal grid size.

Figure 1 shows the comparison between the previous PBL scheme and the new one at 03 UTC (noon) June 5, 2003. The initial time of this experiment is 18 UTC June 4, 2003. By using the new PBL scheme, the mixing length at the lowest level is increased, and the mixing ratio of the water vapor at the lowest level is decreased. Figure 2 shows the time sequence of the temperature and dew-point temperature at 1.5 [m] at Kumagaya. As shown in Figure 2, the Problem 2 is also solved.

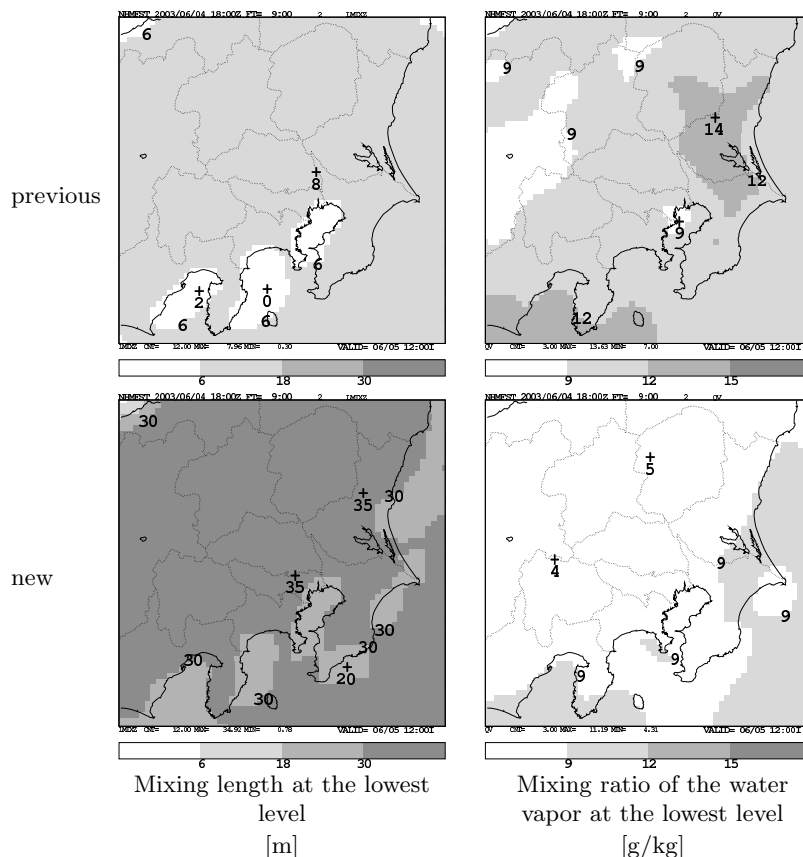


Figure 1: The spatial distributions of the mixing length at the lowest level and the mixing ratio of the water vapor at the lowest level over the Kanto region at 03 UTC June 5, 2003.

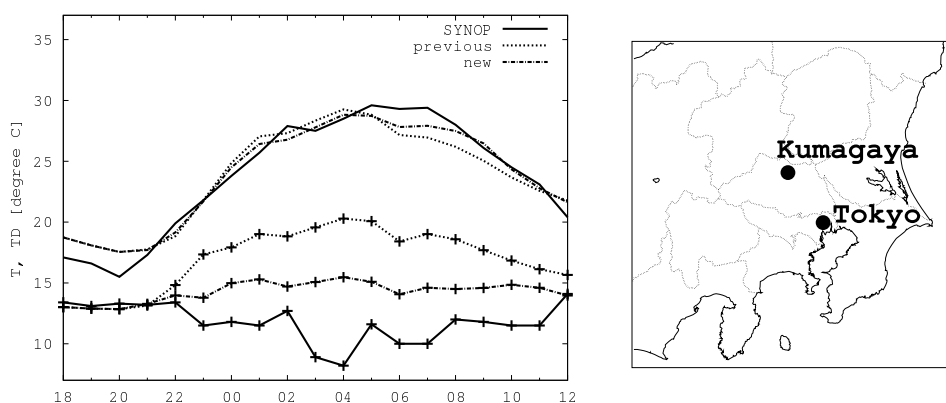


Figure 2: The time sequence of the temperature and dew-point temperature at 1.5 [m] at Kumagaya. The lines and lines with cross dots represent the temperature and dew-point temperature, respectively.

## References

- [1] Kumagai, Y., 2004 : "Improvement of the land surface processes in JMANHM", *CAS/JSC WGNE Research Activities in Atmospheric and Oceanic Modelling*, submitted.
- [2] Sun, W. Y. and C. Z. Chang, 1986 : "Diffusion model for a convective layer. Part I: Numerical simulation of convective boundary layer", *J. Climate Appl. Meteor.*, **25**, 1445 - 1453.

# Improvement of the land surface processes in JMANHM

KUMAGAI Yukihiro

Numerical Prediction Division, Japan Meteorological Agency

1-3-4 Otemachi, Chiyoda, Tokyo 100-8122, Japan, [kumagai\\_y@met.kishou.go.jp](mailto:kumagai_y@met.kishou.go.jp)

The JMA non-hydrostatic model(JMANHM) is a community model which has been developed for use of both operational prediction and research. JMANHM is known to have several problems in the surface properties such as temperature and humidity:

**Problem 1** The cold bias at the surface in case of the unstable conditions.

**Problem 2** The wet bias at the surface.

The causes of the problems are the following points:

**Cause 1** Too much the surface latent heat flux.

**Cause 2** Too small the eddy diffusion coefficients.

The more the surface latent heat flux exists, the more surface cooling occurs. That is why the cold bias at the surface existed. Furthermore, because of the small turbulent mixing with the small eddy diffusion coefficients, the water vapor in the lower model level is accumulated too much. That is why the wet bias at the surface existed.

To remove the Cause 1, the following modifications have been made.

## 1) Scalar roughness lengths

In JMANHM, the roughness length for scalars (heat and moisture) had been the same as that for momentum. Since this treatment tends to overestimate the surface heat and moisture fluxes, the values of the scalar roughness lengths have been reduced following Garratt and Francey[2].

## 2) Methods for calculating the bulk coefficients

In JMANHM, a bulk method is used for calculating the surface fluxes. To calculate the bulk coefficients on the land, an iteration scheme by applying Sommeria[6]'s method had been used. To save the iteration time, the value of the dimensionless height  $\zeta$  had been restricted as follows:

$$-2.5 \leq \zeta \leq 1.5 . \quad (1)$$

Since this restriction does not give satisfactory results for the strongly stable and strongly unstable cases, the following three methods which do not restrict the dimensionless height  $\zeta$  have been implemented into JMANHM:

- method by Businger et al.[1]
- method by Kader and Yaglom[3]
- method by Louis et al.[5]

## 3) Stomatal resistance

The stomatal resistance has been introduced into JMANHM. The stomatal resistance  $r_s$  is controlled by using the downward shortwave radiation flux  $S_{\downarrow}$  as

$$r_s = \frac{r_n}{1 + S_{\downarrow}} + r_d . \quad (2)$$

Here  $r_n$  and  $r_d$  are constants which vary with a season. By using the stomatal resistance, the diurnal variation of stomatal evapotranspiration activity is taken account of and the surface latent heat flux is decreased.

Figure 1 shows the comparison between the previous land surface processes and the new ones at 03 UTC (noon) June 5, 2003. The initial time of this experiment is 18 UTC June 4, 2003. In this experiment, the method by Louis et al.[5] is used for calculating the bulk coefficients of the new land surface processes. By using the new land surface processes, the surface latent heat flux is decreased, and the temperature at 1.5 [m] is increased and the mixing ratio of the water vapor at the lowest level is decreased. Figure 2 shows the time sequence of the temperature and dew-point temperature at 1.5 [m] at Kumagaya. As shown in Figure 2, the Problem 1 is solved, but the Problem 2 remains. Implementation of a new PBL scheme to solve the Problem 2 is another report[4].

## References

- [1] Businger, J. A., J. C. Wyngaard, Y. Izumi and E. F. Bradley, 1971 : "Flux - profile relationships in the atmospheric surface layer", *J. Atmos. Sci.*, **28**, 181 - 189.

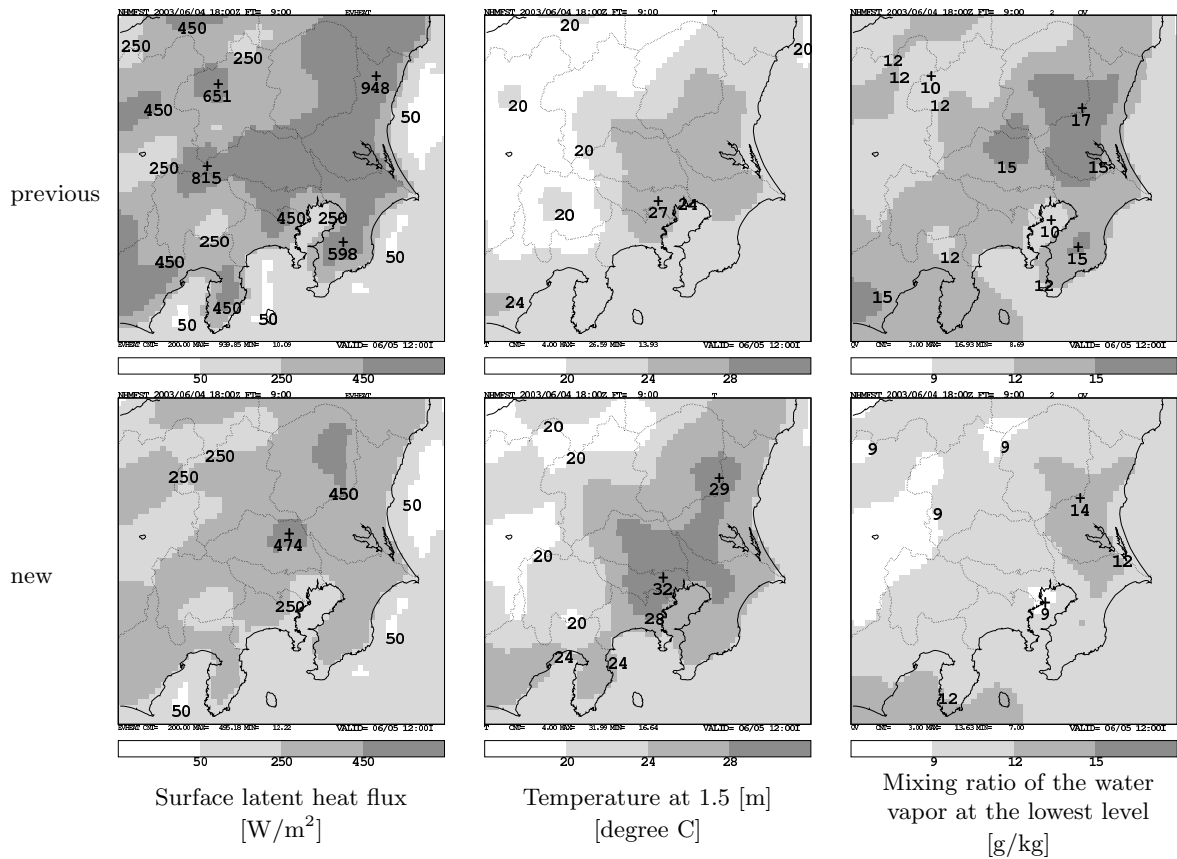


Figure 1: The spatial distributions of the surface latent heat flux, the temperature at 1.5 [m] and the mixing ratio of the water vapor at the lowest level over the Kanto region at 03 UTC June 5, 2003.

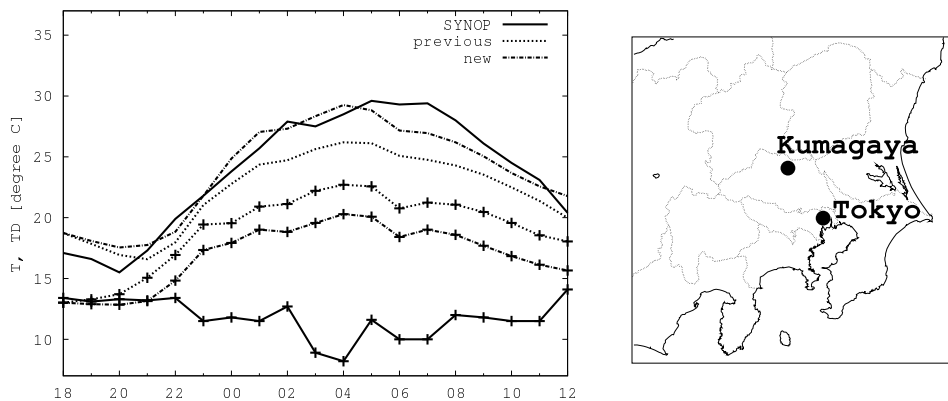


Figure 2: The time sequence of the temperature and dew-point temperature at 1.5 [m] at Kumagaya. The lines and lines with cross dots represent the temperature and dew-point temperature, respectively.

- [2] Garratt, J. R. and R. J. Francey, 1978 : "Bulk characteristics of heat transfer in the unstable, baroclinic atmospheric boundary layer", *Boundary-Layer Meteor.*, **15**, 399 - 421.
- [3] Kader, B. A. and A. M. Yaglom, 1990 : "Mean fields and fluctuation moments in unstably stratified turbulent boundary layers", *J. Fluid Mech.*, **212**, 637 - 662.
- [4] Kumagai, Y., 2004 : "Implementation of a non-local like PBL scheme in JMANHM", *CAS/JSC WGNE Research Activities in Atmospheric and Oceanic Modelling*, submitted.
- [5] Louis, J. F., M. Tiedtke and J. F. Geleyn, 1982 : "A short history of the operational PBL parameterization at ECMWF", Workshop on Planetary Boundary Layer Parameterization, *ECMWF*, England, 59 - 79.
- [6] Sommeria, G., 1976 : "Three - dimensional simulation of turbulent processes in an undisturbed trade wind boundary layer", *J. Atmos. Sci.*, **33**, 216 - 241.

# Testing the new ice model for the global NWP system GME of the German Weather Service

*Dmitrii Mironov and Bodo Ritter*

German Weather Service, Offenbach am Main, Germany<sup>†</sup>

A new ice model (Mironov and Ritter 2003) for the global NWP system GME (Majewski et al. 2002) of the German Weather Service has been tested through parallel experiments including data assimilation. The main features of the new GME ice model are briefly outlined as follows. The model accounts for thermodynamic processes only, i.e. no ice rheology is considered. The heat transfer through the ice is treated using the integral, or bulk, approach. It is based on a parametric representation (assumed shape) of the evolving temperature profile within the ice and the integral heat budget of the ice layer. Simple thermodynamic arguments are invoked to compute the ice thickness. The result is a system of two ordinary differential equations for the two time-dependent quantities, the temperature  $T_i(t)$  at the air-ice interface and the ice thickness  $H_i(t)$ . No snow over the ice is considered at present (although provision is made to account for the snow layer). As regards the horizontal distribution of the ice cover, the ice model is obedient to the GME data assimilation scheme. If a GME grid box has been set ice-free during the initialisation, no ice is created over the forecast period. If observational data indicate open water conditions for a given grid box, residual ice from the model forecast is removed and the water surface temperature is set to the observed value. At present, no fractional ice cover is considered. The GME grid box is treated as ice-covered once the assimilation scheme has detected an ice fraction greater than 0.5. The newly formed ice has the thickness of 0.5 m. Prognostic ice thickness is limited by a maximum value of 3 m.

Results from numerous test runs have shown that the ice surface temperature is rather sensitive to the cloud cover, particularly during winter, and that the ice albedo with respect to the short-wave solar radiation,  $\alpha$ , plays a major part in forecasting  $T_i(t)$ , particularly during summer. The following formulation is proposed for use in GME:  $\alpha = \alpha_{max} - (\alpha_{max} - \alpha_{min}) \exp[-C_\alpha(T_{f0} - T_i)/T_{f0}]$ . Here,  $\alpha_{max} = 0.65$  and  $\alpha_{min} = 0.40$  are maximum and minimum values of the ice albedo, and  $C_\alpha = 95.6$  is a fitting coefficient. The above formulation is meant to implicitly account (in a crude way) for the seasonal changes of  $\alpha$ . During summer, when the ice surface temperature is close to the fresh-water freezing point  $T_{f0} = 273.15$  K, a decrease of the area-averaged albedo occurs due to the presence of meltwater ponds and leads (see e.g. Ebert and Curry 1993). A minimum value of  $\alpha_{min} = 0.40$  is close to the estimates of the wavelength-integrated albedo reported by Ebert and Curry (1993) and Perovich et al. (2002). This value is typical of the summer months in the Arctic.

Figure 1 shows the two-metre temperature in the Arctic, as computed by GME with the new ice model and by ECMWF, versus observations. Recall that the ECMWF ice model solves a finite-difference analogue of the one-dimensional heat transfer equation for the ice slab of fixed depth. The two simulations show a somewhat different spatial temperature structure. The overall agreement of both simulations with data is satisfactory, considering possible uncertainties and sparsity of available observational data. The ice thickness in the Arctic computed with the new GME ice model is illustrated in Fig. 2. The ice thickness distribution looks reasonable. This is difficult to verify quantitatively, however, for lack of observational data.

*Acknowledgements.* The work was partially supported by the EC Project INTAS-01-2132.

---

<sup>†</sup>Corresponding address: Deutscher Wetterdienst, Frankfurter Str. 135, D-63067 Offenbach am Main, Germany. E-mail to [Dmitrii.Mironov@dwd.de](mailto:Dmitrii.Mironov@dwd.de) and [Bodo.Ritter@dwd.de](mailto:Bodo.Ritter@dwd.de).



Figure 1. The two-metre temperature in the Arctic at 12 UTC on 5.12.2003: left panel – GME analysis using the new ice model, right panel – ECMWF analysis. Numbers show computed minus observed two-metre temperature difference (in K).

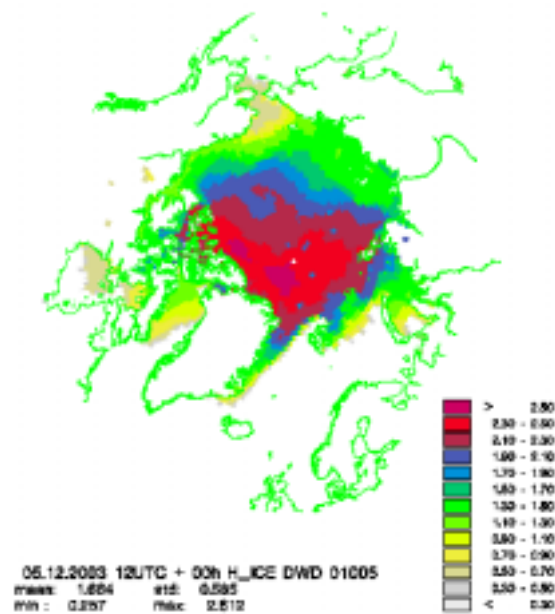


Figure 2. The ice thickness  $H_i$  in the Arctic at 12 UTC on 5.12.2003 computed with the new ice model.

## References

- Ebert, E. E., and J. A. Curry, 1993: An intermediate one-dimensional thermodynamic sea ice model for investigating ice-atmosphere interactions. *J. Geophys. Res.*, **98**, 10,085–10,109.
- Majewski, D., D. Liermann, P. Prohl, B. Ritter, M. Buchhold, T. Hanisch, G. Paul, W. Wergen, and J. Baumgardner, 2002: Icosahedral-hexagonal gridpoint model GME: description and high-resolution tests. *Mon. Weather Rev.*, **130**, 319–338.
- Mironov, D., and B. Ritter, 2003: A first version of the ice model for the global NWP system GME of the German Weather Service. *Research Activities in Atmospheric and Oceanic Modelling*, J. Côté, Ed., Report No. 33, April 2003, 04.13–04.14.
- Perovich, D. K., T. C. Grenfell, B. Light, and P. V. Hobbs, 2002: Seasonal evolution of the albedo of multiyear Arctic sea ice. *J. Geophys. Res.*, **107**, 20-1–20-13.

# A Lake Model for Use in Numerical Weather Prediction Systems

*Dmitrii Mironov<sup>1</sup>, Arkady Terzhevik<sup>2</sup>, Frank Beyrich<sup>1</sup> and Erdmann Heise<sup>1</sup>*

<sup>1</sup> German Weather Service, Offenbach am Main, Germany<sup>†</sup>

<sup>2</sup> Northern Water Problems Institute, Russian Academy of Sciences, Petrozavodsk, Russia

A lake model intended for use in NWP systems (also in climate modelling and other numerical prediction systems for environmental applications) is developed (Mironov 2003). The model is capable of predicting the surface temperature in lakes of various depth on time scales from a few hours to a year. It is based on a two-layer parametric representation of the temperature profile, where the structure of the lake thermocline is described using the concept of self-similarity (assumed shape) of the evolving temperature profile (Kitaigorodskii and Miropolsky 1970). The same concept is used to describe the temperature structure of the thermally active upper layer of bottom sediments and of the ice and snow cover. The proposed lake model incorporates (i) a flexible parameterisation of the temperature profile in the thermocline, (ii) an advanced formulation to compute the mixed-layer depth, including the equation of convective entrainment and a relaxation-type equation for the depth of a wind-mixed layer, (iii) a module to describe the vertical temperature structure of the thermally active layer of bottom sediments and the interaction of the water column with bottom sediments, and (iv) an advanced snow-ice module. Empirical constants and parameters of the proposed model are estimated, using independent empirical and numerical data. They should not be re-evaluated when the model is applied to a particular lake. In this way, the model does not require re-tuning, a procedure that may improve an agreement with a limited amount of data but should generally be avoided.

In order to compute fluxes of momentum and of sensible and latent heat at the lake surface, a parameterization scheme is developed that accounts for specific features of the surface layer over lakes. The scheme incorporates (i) a fetch-dependent formulation for the aerodynamic roughness of the water surface, (ii) advanced formulations for the roughness lengths for potential temperature and specific humidity in terms of the roughness Reynolds number, and (iii) free-convection heat and mass transfer laws to compute fluxes of scalars in conditions of vanishing mean wind.

The new lake model and the new surface air layer parameterization scheme are tested against data through single-column numerical experiments. Figure 1 shows the water surface temperature  $\theta_s$  as computed by the proposed lake model against data from measurements in Kossenblatter See, a shallow lake located in Land Brandenburg, Germany. In Fig. 2, fluxes of sensible  $Q_{se}$  and latent  $Q_{la}$  heat computed with the surface-layer scheme are compared with data from flux measurements in the atmospheric surface layer over the lake. Details of measurements are given in Beyrich (2000). As seen from Figs. 1 and 2, the model predictions show a good agreement with observations. The work is underway to further test the new lake model and the new surface layer parameterization scheme against data from measurements in/over different lakes, and to integrate the lake model and the surface-layer scheme into the full three-dimensional NWP system environment.

*Acknowledgements.* The work was partially supported by the EU Commission through the project INTAS-01-2132.

---

<sup>†</sup>Corresponding author address: Deutscher Wetterdienst, AP2003, Frankfurter Str. 135, D-63067 Offenbach am Main, Germany. E-mail to Dmitrii.Mironov@dwd.de.

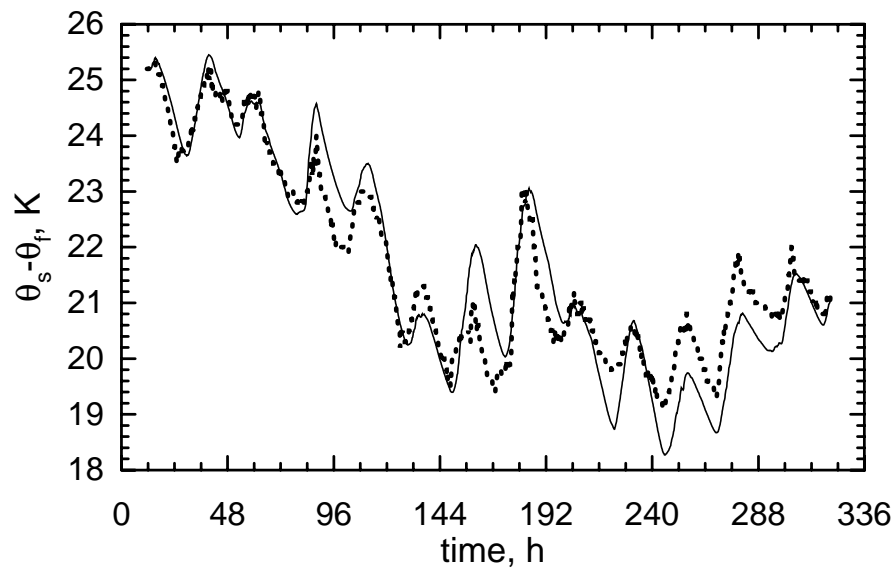


Figure 1. The water surface temperature ( $\theta_f = 273.15$  K is the fresh-water freezing point) computed with the new lake model, solid curve, versus data from measurements in Kossenblatter See over the period from 8 to 21 June 1998, dotted curve.

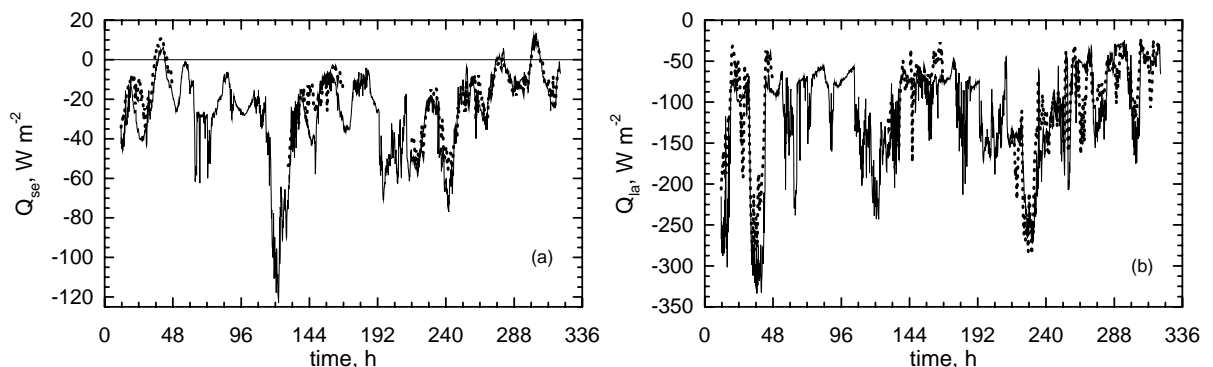


Figure 2. Computed with the surface-layer scheme, solid curves, and measured, dotted curves, fluxes of sensible heat (a) and of latent heat (b) over Kossenblatter See during the period from 8 to 21 June 1998.

## References

- Beyrich, F., (Ed.), 2000: *LITFASS-98 Experiment. 25.5.1998 – 30.6.1998. Experiment Report. Arbeitsergebnisse Nr. 62*, Deutscher Wetterdienst, Geschäftsbereich Forschung und Entwicklung, Offenbach am Main, Germany, 78 pp.
- Kitaigorodskii, S. A., and Yu. Z. Miropolsky, 1970: On the theory of the open ocean active layer. *Izv. Akad. Nauk SSSR. Fizika Atmosfery i Okeana*, **6**, 178–188.
- Mironov, D. V., 2003: Parameterization of lakes in numerical weather prediction. Part 1: Description of a lake model. In preparation.

# Implementation of the Kain-Fritsch Convective Parameterization scheme in the JMA's Non-hydrostatic Model

Shiro Ohmori and Yoshinori Yamada

*Numerical Prediction Division, Japan Meteorological Agency  
1-3-4 Otemachi, Chiyoda-ku, Tokyo 100-8122, Japan  
E-mail: s-ohmori@met.kishou.go.jp*

## 1. Introduction

A mesoscale non-hydrostatic model (JMA-NHM hereafter) is being developed at JMA for operational use. The model includes an explicit mixed-phase three-class bulk microphysical model, in which mixing ratios and number concentrations of water substances are predicted. In the early stage of its operation, a horizontal resolution of 10km and relatively longer time step of about 40 seconds are expected. It was, however, found from preliminary experiments that a convective parameterization scheme should be jointly employed in order that the stability of the model is assured, and that representation of relatively weak precipitation is good enough. Even though the JMA-NHM has been equipped with two convective parameterization schemes (Arakawa-Schubert and moist convective adjustment schemes), the Kain-Fritsch convective parameterization scheme (Kain and Fritsch 1990, hereafter K-F CPS) based on the convective available potential energy (CAPE) seems to be appropriate because the model under development will be executed in a region at midlatitude, where CAPE is closely related to the convective activities. In addition, the K-F CPS is designed to work well in models with finer resolutions.

The parameterization code of the K-F CPS as of Apr. 2002 for the Eta model is provided from the WRF (Weather Research and Forecasting) model with permission of Dr. Kain (Yamada 2003). Minor improvements of the K-F CPS made in February 2003 (Kain 2002) have also been reflected in the K-F CPS incorporated in the JMA-NHM. The original code has a high performance in the Eta model with a 25km resolution, its performance in the JMA-NHM with a 10km resolution is, however, not very good regarding precipitation representation. Thus, adjustments of the original parameterization code have been made in order to obtain sufficient performance in the JMA-NHM with such finer resolution of around 10 km. These adjustments may be natural because the parameterization depends on the three-dimensional thermodynamical structures of the model atmosphere.

This paper describes adjustments of the K-F CPS and a new precipitation formation scheme for reproducing precipitation fields satisfactorily.

## 2. Adjustments of the parameterization

Since the original parameterization code of the K-F CPS didn't give good results in precipitation forecasts as mentioned above, adjustments of the scheme important to the improvement of its performance are made in its three major components, namely "trigger function", "updraft property", and "closure assumption".

In the "trigger function", a concept of temperature increment is introduced as in Fritsch and Chappell (1980) to simulate local perturbation forcing as a function of grid-scale motion. Even though this temperature increment is formulated in the original K-F CPS code as a function of horizontal grid resolution, a value from this formulation may be too large for 10km horizontal resolution, leading to producing undesirable rainfall in regions where no precipitation was observed. Thus, the increment of temperature is reduced by a certain amount of the values determined in the K-F CPS in the original code.

As for the calculation of "updraft property", precipitation is continuously produced in the updraft regardless of the content of condensates by a method proposed by Ogura and Cho(1973). With this precipitation formation scheme, unnatural precipitation patterns were sometimes obtained such as elongated precipitation regions whose orientations were perpendicular to those of major rain bands. In order to ameliorate such precipitation patterns, a new precipitation scheme is introduced; this new scheme will be explained in the next section.

Concerning the "closure assumption", the default setting is assumed that the convection consumes the pre-existing CAPE by 90%. Forecast experiments showed that this closure assumption tends to considerably stabilize the model atmosphere, especially at around the

end of forecast period of 15 and 18 forecast hours. Accordingly, the consumption of CAPE is changed.

### 3. New scheme for precipitation formation in the K-F CPS

In order to improve the aforementioned precipitation patterns, a new scheme of precipitation formation is introduced. This new scheme is based on the concept of the Kessler type autoconversion scheme, that is, the condensates in the updraft are converted into precipitation only when their condensates exceed a prescribed value. This scheme functions fairly well, and is now used taking the place of the Ogura and Cho (1973) scheme.

### 4. Forecast experiments

Forecast experiments of a heavy rain fall event, which occurred on 20 July 2003 over Kyushu Island, western part of Japan, are conducted by the JMA-NHM of 10km resolution in order to compare performance of the adjusted K-F CPS to that of the original one. In this event, a maximum rain rate reached 81mm hr<sup>-1</sup>, and three hourly accumulated rain was 142 mm. In these experiments, a mixed-phase three-class bulk microphysical model, in which mixing ratios of water substances are predicted, are employed in conjunction with the K-F CPS.

With the adjusted K-F CPS, heavy rain fall is well reproduced (Fig.1a) over Kyushu Island, consistent with observations (Fig.1b). On the contrary, the original K-F CPS gives relatively weak rain fall spread over and around Kyushu Island (Fig.1c).

### 5. Future Plan

In the present K-F CPS, occurrence of convection is diagnosed by forecast variables at each grid. This may lead to form convective precipitation at a scale of grid resolution. Thus, it is planned to use forecast variables averaged over horizontal scale 30km to diagnose an occurrence of convection.

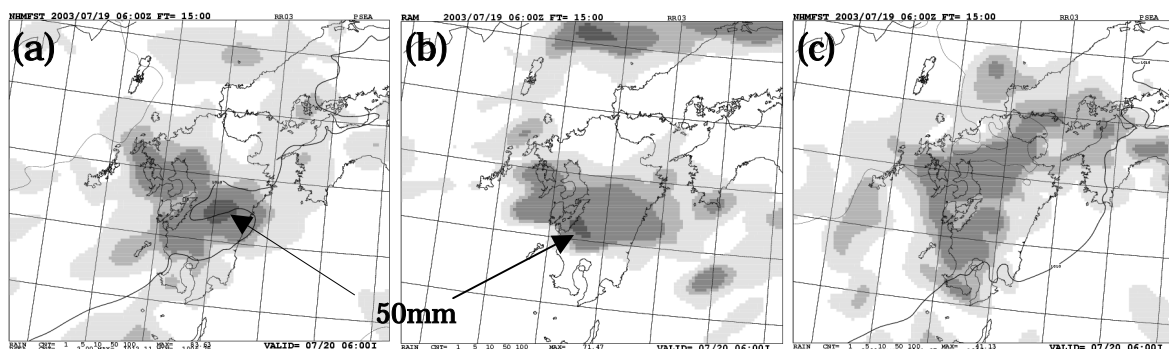


**Fig. 1.** (a) Three hourly accumulated precipitation(mm) in between forecast hours from 12 to 15 with the adjusted K-F CPS. Initial time for forecast experiments is 06UTC July 19 2003. The accumulated rain amount is depicted by shading of four levels indicating 1-5mm, 5-10mm, 10-50mm, and over 50mm from the most light shading. (b) Three hourly accumulated rain derived from radar data corrected by rain gauge data in the period corresponding to Fig.1a. (c) As in Fig.1a, but with the original K-F CPS.

### References

- Fritsch, J.M. and C. F. Chappell, 1980: Numerical prediction of convectively driven mesoscale pressure systems. Part : Convective parameterization. *J. Atmos Sci.*, 37, 1722-1733.
- Kain, J.S., and J.M. Fritsch, 1990: A one-dimensional entraining/detraining plume model and its application in convective parameterization. *J. Atmos Sci*, 47, 2784-2802.
- Kain, J.S., 2002: The Kain-Fritsch Convective Parameterization: An Update. *Submitted to J. Appl Meteor.*
- Ogura, Y. and H.-R. Cho, 1973: Diagnostic determination of cumulus cloud populations from observed large-scale variables. *J. Atmos. Sci.*, 30, 1276-1286.
- Yamada, Y. 2003: Cumulus Convection Schemes. *Suuchiyohou-ka Houkoku Bessatsu* 49, 84-89.(in Japanese)

# HYDRODYNAMIC AND STATISTICAL MODEL OF OPERATIVE FORECAST TO 36 H AHEAD OF DANGEROUS SUMMER WIND INCLUDING SQUALLS AND TORNADOES IN THE EUROPEAN PART OF RUSSIA AND IN EUROPE

E.V.Perekhodtseva – Hydrometeorological Center of Russia, B.Predtechenskii 9-13, Moscow, Russia

Development of successful method for automated statistical forecast of heavy rainfalls, as well as strong summer winds, including squalls and tornadoes, that often result in human and material losses, could allow one to take proper measures against destruction of buildings and to protect people. Well-in-advance forecast (from 12 hours to two days) of heavy rainfalls makes possible to take proper measures against floods and to reduce the losses. Prediction of the phenomena involved is a very difficult problem for synoptic till recently. The existing graphic and calculation methods still depend on subjective decision of an operator.

At the present time in Russia there is no hydrodynamic model for forecast of heavy rainfalls and the maximal speed of wind, hence the main tools of objective forecast are statistical methods using the dependence of the phenomena involved on a number of atmospheric parameters (predictors).

Successful development of hydrodynamic models for short- and mid-term forecast and improvement of two-three-day forecasts of pressure, temperature and others parameters allow us to use the prognostic fields of those models for calculations of the discriminant functions in the nodes and the values of probabilities of dangerous precipitation and winds and thus to get fully automated forecasts. Statistical decisive rules for the alternative and probability forecasts for each of the phenomena involved were obtained in accordance with the concept of “perfect prognosis” using the data of objective analysis. For this purpose the teaching samples were automatically arranged that include the values of forty physically substantiated potential predictors.

Then the empirical statistical method was used that involved diagonalization of the mean correlation matrix of the predictors and extraction of diagonal blocks of strongly correlated predictors. Thus for each phenomena the most informative predictors were selected without losing information, those predictors being either a representative of each block or an independent informative predictors. The statistical decisive rules for diagnosis and prognosis of the phenomena involved were calculated for the most informative vector-predictor that includes the most informative (we used the criterion of distance of Mahalanobis and criterion of minimum of entropy by Vapnik-Chervonenkis) and slightly dependent predictors.

For prognosis of the phenomena involved with the given advance period the values of the discriminant functions and the probabilities of the phenomena were calculated using the prognostic values of the hemispherical model in the nodes of the rectangular mesh 150x150 km over the European part of Russia and Europe. In order to change to the alternative forecast the author proposes the empirical threshold values specified for each phenomena and advance period.

According to the Pirsey-Obukhov criterion (T), the success of the 24-hour forecast and the method of forecast of dangerous precipitation in the warm season for the first and second day, as used in Hydrometeorological Center of Russia since 1998 as the main calculation method, is  $T=0,49-068$ . The same is true for the forecast of dangerous squalls and tornadoes, that was tested by Hydrometeorological Center of Russia in 1999-2000 and was included into the automatic prognosis system in the summer of 2001. The method for forecast of very dangerous precipitation (the quantity over 50 mm/12h ) was tested successful in some regions of European part of Russia in 1998-2002 .

The forecast of strong summer wind with the value of velocity over 25m/s is developed for next day and next night to 36 hours ahead and is included into operative system of Hydrometeorological Center of Russia. Nowadays this forecast is produced two times per day as the help tool for a synoptic.

# Improved hydrodynamical scheme of the turbulence description

**Shnaydman V.A.**

**Department of Environmental Sciences, State New Jersey University-Rutgers,  
Cook college, 14 College Farm Rd, New Brunswick, NJ, 08901 USA,  
e-mail: volf@envsci.rutgers.edu**

The quantitative description of the turbulence is one of the problems in the current prediction of the large and mesoscale atmospheric processes. The prediction schemes use the equations of resolved scales of hydrodynamic variables and subgrid simulation model of turbulence characteristics for unresolved scales.

The most popular hydrodynamic description of atmospheric turbulence is based on the Level-3 and Level-2.5 model according to the classification of Mellor-Yamada [5,6]. The difference between these two models is that the Level-3 model uses two transport equations for turbulent kinetic energy (TKE) and temperature variance while the Level-2.5 includes only the transport equation for TKE and algebraic expressions for all second-moments of the fluctuations of variables. The greatest weakness of the hydrodynamic schemes based on Level-3 and Level-2.5 models is that they are constructed by using the conception of master length scale. This scale is calculated by the empirical expression, it's for example the formulae of Blackadar-Deardorff [4,6].

We developed the hydrodynamic model with two transport equation closure TKE and dissipation rate which was used for reconstruction internal structure of atmospheric boundary layer from operational data of Hydrometeorological Center of Russia. The arguments in favor of using this hydrodynamic model is shown [1,2].

The proposal improvement is the Level-3 model but the transport equation of dissipation rate is applied instead of the transport equation of the temperature variance. The expression for length scale is constructed by using the formulae of Kolmogorov-Prandtl (KP) with the predicted turbulence characteristics (TKE and dissipation rate). The obtained results show that less turbulent energy is transferred to the smallest eddies and dissipation decreases faster than  $(TKE)^{\frac{3}{2}}$  when the stratification parameter increases. Therefore the value of length scale decreases if the stratification is unstable and increases when the stratification becomes stable [3,4]. In improved scheme the algebraic expressions for the second moments are transformed by using KP formulae for length scale. This value fits the balance described by TKE transport equation. The pressure-velocity and pressure- temperature correlations are also included in the algebraic expressions as it recommended in [4]. So the all

components of the turbulent fluxes of momentum and heat are obtained. These fluxes are inserted in the equations for components of mean velocity and mean potential temperature in the prediction model.

The developed hydrodynamic scheme is also used for modeling the transport and diffusion of hazardous releases and can be applied for creation of an operational tool for real-time air pollution monitoring. For solution this problem the developed scheme is used to calculate the coefficients of turbulence, which are involved in the equation of turbulent diffusion of the pollutants. The calculation of the turbulence coefficients is based on the obtained algebraic expression of the second moments. The obtained expression of the turbulence coefficients has the same form as KP formulae but it includes the stability functions, which are depended from TKE, dissipation rate, the wind shear and the potential temperature gradient. The calculated and defined in [4] stability functions are different because the calculated ones don't require the empirical expression for length scale. So the proposed algorithm is more physically well-grounded than the constant values of the proportionality coefficient in KP expression [1].

The improvement allows to include the scheme for description of the turbulent exchange on the whole calculation domain of forecast model.

The application of developed scheme for turbulence description to the forecast models and pollution modeling gets better the quality of weather prediction and ecological monitoring.

#### References:

1. Berkovich, L.V., Tarnopolskii, A.G., Shnaydman, V.A.: 1997, "A Hydrodynamic Model of the Atmospheric and Oceanic Boundary Layers," Russian Meteorology and Hydrology 7, 30-40.
2. Berkovich, L.V., Tarnopolskii, A.G., Shnaydman, V.A.: 1998, "Reconstruction of the Internal Structure of the Atmospheric Boundary Layer from Operational Meteorological Data," Russian Meteorology and Hydrology 7, 22-31.
3. Cheng Y., and Canuto, V.M.: 1994,"Stably Stratified Shear Turbulence: A New Model for the Energy Dissipation Length Scale", J.Atmos. Sci., 16, 2384-2396.
4. --, --, and Howard, A.M.: 2001,"An Improved Model for Turbulent PBL", J.Atmos. Sci., 59, 1550-1565.
5. Mellor, G.L., and T. Yamada, 1974:"A Hierarchy of Turbulence Closure Models for Planetary Boundary Layer", J.Atmos. Sci., 31,1791-1806.
6. --, and --, 1982: "Development of Turbulent Closure Model for Geophysical Fluid Problems", Rev. Geophys. Space Phys., 20, 851-875.

# Variable-lag Channel Flow Routing Algorithm for climate models

Sushama, L., R. Laprise<sup>1</sup>, D. Caya<sup>1, 2</sup>, M. Larocque<sup>1</sup> and M. Slivitzky<sup>2,3</sup>

<sup>1</sup>Département des Sciences de la Terre et de l'Atmosphère

Université du Québec à Montréal

<sup>2</sup>Ouranos, <sup>3</sup>INRS-EETE, C.P. 7500, Sainte-Foy, Québec, Canada, G1V 4C7

E-mail: sushama@sca.uqam.ca

## 1. Introduction

In the climate modeling community, there is a need for models that can route runoff generated by the land surface component of Global Circulation Models (GCMs) and Regional Climate Models (RCMs) to the ocean cells of the ocean-modeling component as the fresh water influx is an important buoyancy source for coastal ocean circulation. Routing models are also required to fully evaluate the impact of climate change on water resources. A simple cell-to-cell routing scheme based on Askew's formula (1970) and the findings of Boyd (1981) and Kumar *et al.* (1997) for computing time-evolving channel lags is implemented.

## 2. Model

The control volume in cell-to-cell routing is the grid cell. Each grid cell is conceptualized as a watershed with two reservoirs, the surface and groundwater reservoirs, as in the variable-velocity scheme of Arora and Boer (1999). The water balance within each grid cell for the surface and groundwater stores are given by continuity equation as

$$\begin{aligned} \frac{dS}{dt} &= I - Q; \\ \frac{dG}{dt} &= f_p - f_g, \end{aligned} \quad (1a, 1b)$$

where  $S$  and  $G$  are the surface water and groundwater stores respectively.  $I$  and  $Q$  are the inflow and outflow respectively for the surface water store.  $I$  is the sum total of the surface runoff generated within the grid cell ( $f_s$ ), the flow from neighboring cells ( $f_n$ ) and the contribution from the ground water store ( $f_g$ ) of the same grid cell, i.e.

$$I = (f_s + \sum_n f_n + f_g). \quad (2)$$

$f_p$  is the inflow into the groundwater store. Both surface water and groundwater stores are modeled as linear reservoirs, i.e. the surface water and groundwater stores are assumed to be related linearly to their outflows as

$$S = kQ; \quad G = k_g f_g. \quad (3a, 3b)$$

The channel lag  $k$  is the travel time between the grid cell under consideration and its downstream neighbor. Based on the findings of Boyd (1981) and Kumar *et*

*al.* (1997), the channel lag  $k$  in hours can be approximated by

$$k = 0.6 \square K, \quad (4)$$

where  $K$ , the basin lag (in hours), is given by Askew's formula,

$$K = \square A^\square Q^\square. \quad (5)$$

In Eq. (5),  $A$  is the basin area (in km<sup>2</sup>),  $Q$  is the flow rate in (m<sup>3</sup>s<sup>-1</sup>), and  $\square$ ,  $\square$  and  $\square$  are constants ( $\square = 2.12$ ,  $\square = 0.57$  and  $\square = -0.23$ ). The residence time associated with the groundwater reservoir,  $k_g$ , is assumed to be related to the major soil type of the grid cell as in Arora and Boer (1999).

Basin discretization and flow directions for the routing scheme are adapted from global data sets of continental watersheds and river networks of Graham *et al.* (1999). In the absence of gridded estimates of observed daily runoff, the runoff fields from the Variable Infiltration Capacity (VIC) hydrological model (Lohmann *et al.* 1998) is used.

## 3. Results

Routing is performed for Mississippi and Fraser basins at 5 min resolution. The choice of the routing time interval is very critical and varies with spatial resolution as in any hydrological model. Knowing the area of the cell at the basin outlet and the range of flows expected, channel lags corresponding to the range of flows for that particular cell can be computed using Eqs. (4) and (5). Cells located at the mouth have maximum flows and hence the smallest channel lag of all cells in the basin. A suitable choice for the routing interval for the basin would be a value close to the smallest channel lag or response time. The channel lags for the cell at the outlet of the Mississippi and Fraser basins are as in Fig. 1.

As per the scatter plot the channel lag for Mississippi is between one and two hours and that of Fraser between one and three hours at 5 min spatial resolution. Choice of higher routing interval at 5 min spatial resolution will result in delays, with the time to peak of the hydrograph at the mouth of the basin lagged and the peak attenuated as in Fig. 2. The difference in volume between the observed and simulated flows for the Fraser basin (Fig. 2) can be

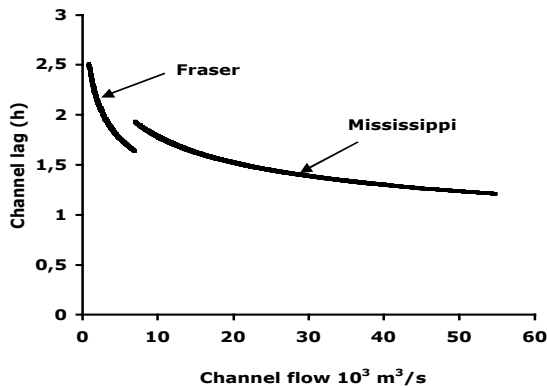


Figure 1. Scatter plot of Channel lag vs. Channel flow for Mississippi and Fraser, at 5 min spatial resolution.

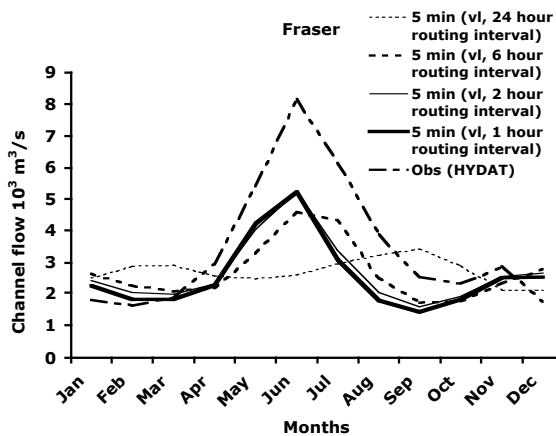


Figure 2. Mean annual hydrographs for Fraser basin at 5 min spatial resolution, for various routing intervals.

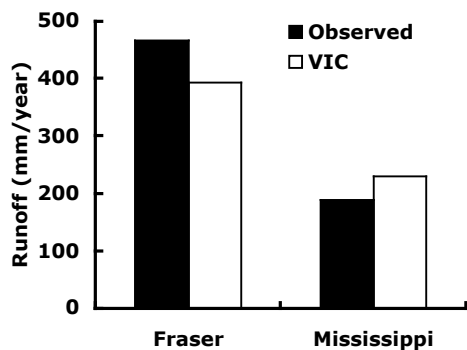


Figure 3. Basin-wide average runoff from observation and VIC data.

partially attributed to the underestimation of runoff (Fig. 3) by the VIC model over Fraser along with the lack of representation of cold region processes.

For the Mississippi basin, the model does a good job in capturing the seasonality (Fig. 4) and the efficiency of the model is quite good. The VIC model overestimates runoff over Mississippi (Fig. 3) and accounts for the difference between the observed and simulated hydrographs.

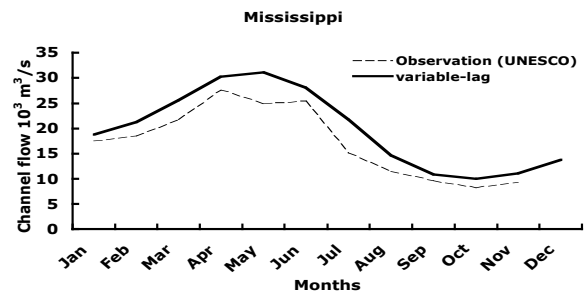


Figure 4. Observed and simulated mean annual hydrograph for the Mississippi basin.

#### 4. Conclusions

The variable-lag routing scheme does a good job in capturing not only the seasonality, but also in simulating the time to peak and volumes. The scheme could be very useful at fine resolution, where the uncertainty associated with parameters can be quite large. The computational efficiency of the scheme is also higher than other routing schemes.

#### References

1. Arora, V. K., and Boer, G. J. (1999) A variable velocity flow routing algorithm for GCMs, *J. Geophys. Res.*, 104, D24, pp. 30965-30979.
2. Askew, A. J. (1970) Derivation of formulae for variable lag time, *J. Hydrol.*, 10, PP. 225-242.
3. Boyd, M. J. (1981) Proceedings of the International Symposium on Rainfall-Runoff Modeling, Edited by Vijay P. Singh, pp. 111-124.
4. Graham, S. T., J. S. Famiglietti, and D. R. Maidment (1999), Five-Minute, 1/2°, and 1° Data Sets of Continental Watersheds and River Networks for Use in Regional and Global Hydrologic and Climate System Modeling Studies, *Water Resour. Res.*, 35(2), pp. 583-587.
5. Kumar, N., K. C. Swain and P. Anand Raj (1997) Proceedings of International symposium on emerging trends in Hydrology, Roorkee, 25-27 September 1997, pp. 603-612.
6. Lohmann, D., A. Raschke, B. Nijssen and D. P. Lettenmaier (1998) Regional scale hydrology: I. Formulation of the VIC-2L model coupled to a routing model, *Hydrol. Sci.*, 43(1), pp. 131-141.

## **Application of steering weight concept to Typhoon Saomai (2000)**

Mitsuru Ueno and Akihiko Murata

Typhoon Research Department, Meteorological Research Institute

e-mail: mueno@mri-jma.go.jp

Tropical cyclone (TC) motion is one of the most important forecasting issues both in the numerical weather prediction (NWP) and operational forecasting. Even with the state-of-the-art NWP models significant disagreements can be sometimes observed in TC track forecast among them although it has been believed that TC movement is primarily determined by the large-scale flow field and therefore should be well predicted with such models.

In an attempt to diagnose the mechanism by which a typhoon moves through vertically sheared environmental flows with keeping its vertical coherency, a series of idealized numerical simulations of typhoon are carried out and eventually a new approach termed "steering weight concept" is proposed based on the numerical results (Ueno 2003). The steering weight is a set of weighting factors numerically derived from the surface pressure tendency equation and can be a measure of the relative contribution of the steering flow at each vertical level to the storm motion. The weight varies significantly depending on the simulated storm structure, and is somewhat inherent to the convection scheme used, while it is found to be robust against the change of environment specified. The overall movements of simulated typhoons are well explained by taking into consideration not only so called "steering flow" but also the steering weight, suggesting that the diversity of simulated tracks is partly attributable to that of the weight.

In this paper the new approach is applied to one of the real typhoon cases, that is, the case of Typhoon Saomai in 2000, to confirm the validity of the concept in real situations. The forecast experiments are performed using a 20km version of the Meteorological Research Institute / Numerical Prediction Division unified nonhydrostatic model with an Arakawa-Schubert cumulus parameterization scheme (AS) or an explicit moisture scheme only (EX). The model uses so-called  $z^*$  coordinate in the vertical and therefore the model variables are defined on constant height surface over the sea. It is found from the experiment that the simulated motion of Saomai is sensitive to and systematically changed with the tuning parameters included in the convection scheme such as entrainment rate and relaxation time, in a consistent manner with the foregoing idealized simulations. When the new approach is applied to the model results, all the simulated tracks are well reproduced by the combination of the respective steering weight and steering flow.

Unlike the foregoing study in which the model variables are defined on sigma surface, the steering weight in the present study is calculated in a straightforward manner. Figure 1 shows the vertical profile of the steering weight averaged over the integration period of 39 hours for two extreme track cases (AScntl and EX) obtained from the forecast experiment. The profiles seem reasonable in that the weight is very small at the very high levels near the tropopause, which is consistent with previous observational studies. Once the steering weight is obtained, the steering motion component is easily computed using the steering flow which is defined as an areal-mean asymmetric flow near the storm center. Figure 2 compares the track reproduced from the steering motion component (SW) with "actual" one which is obtained as successive

MSLP center locations. To see the impact of steering weight on the reproduced track, the track obtained from the conventional deep-layer-mean-flow approach (DLMF) is shown in the figure, in which the steering motion component is defined as the pressure-weighted 850-300 hPa depth-averaged mean flow. The close proximity of DLMF track to SW one in the EX experiment is due primarily to a highly barotropic structure of the simulated steering flow.

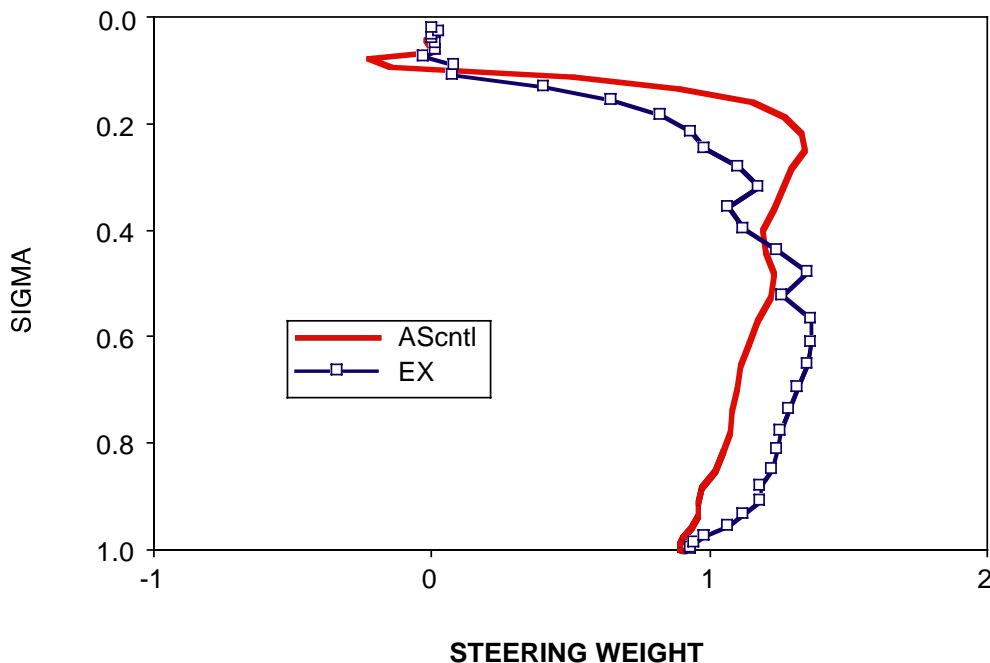


Figure 1: Vertical profile of steering weight.

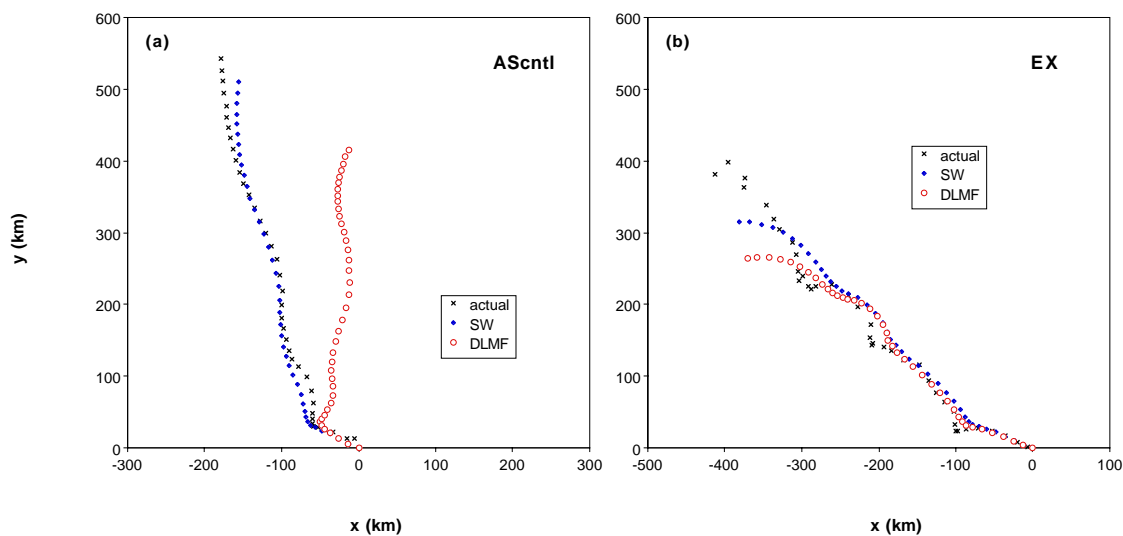


Figure 2: Vortex tracks reproduced from velocity components for (a) ASctl and (b) EX. The vortex is placed at (0,0) initially and symbols indicate hourly positions.

### Reference

Ueno, M., 2003: Steering weight concept and its application to tropical cyclones simulated in a vertical shear experiment. *J. Meteor. Soc. Japan*, **81**, 1137-1161.

# The Effect of Convective Parameterization On Tropical Cyclone Motion and Intensity

XIAQIONG ZHOU<sup>1\*</sup>, JOHNNY C L CHAN<sup>2</sup> AND CHENXI WANG<sup>1</sup>

<sup>1</sup> Shanghai Typhoon Institute, China Meteorological Administration

<sup>2</sup> Laboratory for Atmospheric Research

Department of Physics and Materials Science, City University of Hong Kong

\*Email: [zhouxq@mail.typhoon.gov.cn](mailto:zhouxq@mail.typhoon.gov.cn)

## 1. Introduction

Stensrud et al. (2000) showed that an ensemble with different model physics could give more improvements in short-term forecasts than that from perturbations of initial conditions due to a larger ensemble spread. In this study, the effects of uncertainties in tropical cyclone (TC) model physics on TC forecasting are investigated by comparing the sensitivity results from different convective parameterization schemes and different values of the parameters in the schemes.

## 2. Sensitivity experiments

A nonhydrostatic version of Pennsylvania State University-National Center for Atmospheric Research Mesoscale Model Version 5 (MM5) is used in this study. The domain of 301×301 points has a horizontal grid spacing of 15 km with 23 vertical sigma levels. All experiments are run on a beta plane in a resting environment with a TC bogus using the Typhoon Model of the Japan Meteorological Agency. Four different convective parameterization schemes are used: Betts-Miller (BM), Anthes-Kuo (AK), Grell and Kain-Fritsch (KF) schemes.

## 3. Results

### a) Track forecasts from the four schemes

The 72-h track forecasts from the four convective parameterization schemes show that the position difference between any two convective schemes can be quite significant, especially at long forecast times (Fig. 1a). The northwestward movement of the TC is fastest in the AK scheme while those for the other three schemes are quite similar. The intensities from the four schemes also differ (Fig. 1b). The TC in the BM and AK schemes intensifies rapidly from 990 to 953 hPa in the first 24 h, then weakens in AK but maintains a similar intensity in the BM scheme. In contrast, the TC intensities in KF and Grell are generally lower.

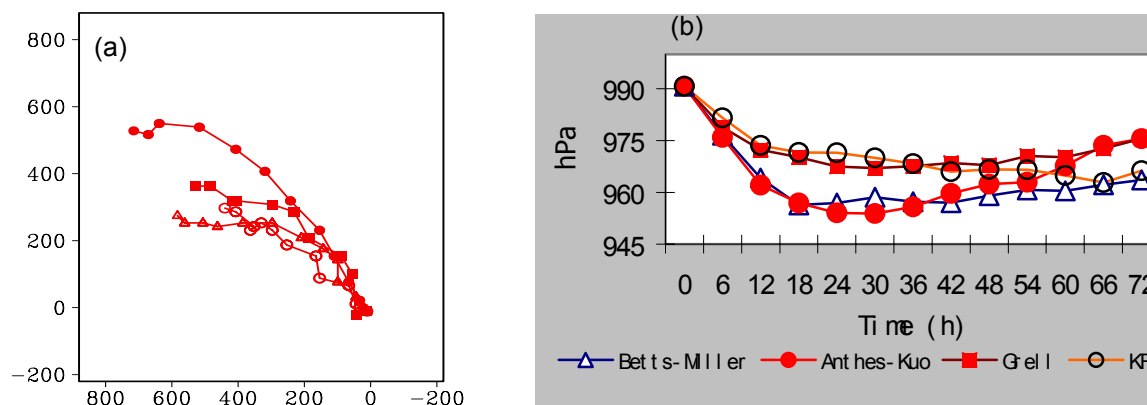


Fig. 1. Predicted (a) tracks, and (b) minimum sea level pressure (MSLP) of TCs using four convective parameterization schemes.

#### b) Changing the parameters in AK and BM schemes

The AK and BM schemes are chosen to study the kind of uncertainty associated with some crucial parameters in the schemes by perturbing their values.

In the AK scheme, convection is determined by the vertically-integrated moisture convergence. Three parameters can be perturbed: the threshold value  $Mt$  of the vertically integrated moisture convergence used to check if convection is possible, the vertical profiles of heating  $Nh$  and a parameter  $b$  that determines the moistening amount and the condensing and precipitating parts. The  $b$  parameter is found to have almost no effect on TC motion but the TC intensity is sensitive to its value (not shown). For the convective heating profile,  $Nh$ , the position of the maximum in the upper half of the cloud is perturbed. When the maximum is rooted in the middle of the cloud instead in the upper level as in the control, the TC position is 300 km east and the MSLP at the TC center is 10 hPa less than that in the control at 72 h. A relative small perturbation to the value of  $Mt$  also causes a divergence in the forecasts of TC movement and intensity.

The BM scheme is based on the simultaneous relaxation of temperature and moisture fields towards the observed quasi-equilibrium thermodynamic structure. The adjustment time scale  $\tau$ , saturation pressure departure and the instability parameter  $a$  (that determines the slope of the temperature profile in relation to the virtual equivalent potential temperature isopleth) are changed according to the sensitivity experiments in Betts (1986a, b). The adjustment time scale for determining the lag of the convective response to large-scale forcing is 50 mins in the control; no obvious effect can be seen when a perturbation of 20 mins is added to or subtracted. A negative perturbation of a relative small value (0.1) of the instability parameter  $a$  has greater effect than a positive one, with the former producing a faster northwest movement than the control but no apparent change in the latter. The effect on intensity is also similar. Saturation pressure departure is closely related to subsaturation, and changing it alters the equilibrium relative humidity. A perturbation value of 10 hPa gives a forecast MSLP difference is  $\sim 10$  hPa while the forecast position has a  $\sim 300$  km difference.

#### 4. Discussion

Results from these sensitivity experiments suggest that uncertainties in the physics in the convective parameterization schemes and in the values of some parameters in these schemes can have significant effects on the forecast of TC intensity and movement. These uncertainty factors should be considered in TC ensemble forecasting. How these factors influence the intensity and movement of TC will also be the subject in the later study.

*Acknowledgments.* This study is supported by the Natural Science Foundation of China Project 40005003 and the Research Grants Council of the Hong Kong Special Administrative Region, China Project CityU 1015/01P.

#### References

- Betts, A. K., 1986a: A new convective adjustment scheme, Part I: observational and theoretical basis. *Quart. J. Roy. Meteor. Soc.*, **112**, 677-691.
- Betts, A. K., 1986b: A new convective adjustment scheme, Part II: Single column tests using GATE, BOMEX, ATEX and arctic air-mass data sets. *Quart. J. Roy. Meteor. Soc.*, **112**, 693-709.
- Stensrud, D. J., J. W. Bao and T. T. Warner, 2000: Using initial condition and model physics perturbations in short-range ensemble simulations of mesoscale convective system. *Mon. Wea. Rev.*, **128**, 2077-2107.